Electron Transport in Amorphous Silicon

A Thesis

Presented to

The Division of Mathematics and Natural Sciences

Reed College

In Partial Fulfillment

of the Requirements for the Degree

Bachelor of Arts

Zachary C. Holman

May 2005

HANWHA 1018

Approved for the Division

(Physics)

John Essick

ACKNOWLEDGEMENTS

Special thanks to John Essick for his advising and experimental expertise, David Cohen for donating the samples, my parents for making a Reed education possible, and Lara Sands for editing this work, putting up with me when I talked about nothing else, and giving me a mullet and a mohawk.

TABLE OF CONTENTS

1 Introduction 1

1.1 Motivation 1

1.2 Scope of this thesis 2

2 Semiconductor Primer 5

2.1 Band structure 5

2.2 Conductivity 7

2.3 Charge generation 9

2.3.1 Thermal excitation 9

2.3.2 Photoexcitation 14

2.4 Charge transport 15

2.5 Crystalline vs. amorphous 19

2.6 Doping 23

2.7 Junctions 24

3 Theory 29

3.1 Overview 29

3.2 Assumptions 30

3.3 Recovering $\psi(t)$ 33

3.4 Short times 34

3.4.1 Electron occupation 34

3.4.2 Transient mobility 38

3.4.3 Photocurrent 39

3.5 Long times 41

3.6 High temperatures 42

3.7 Transit time 44

4 Experimental Methods 47

4.1 Overview 47

4.2 Equipment 49

4.2.1 Laser 49

4.2.2 Optics 50

4.2.3 Bias voltage 51

4.2.4 Oscilloscope 52

4.2.5 Computer 52

4.2.6 Temperature control 52

4.3 Samples 53

5 Results 57

5.1 Qualitative observations 57

5.2 Transient mobility 61

5.2.1 Finding Q_0 63

5.2.2 Normalized current traces 67

5.3 Fitting charge curves 69

6 Conclusion 77

A Detailed Balance 79

References 83

LIST OF FIGURES

1.1 Time-of-flight measurement technique 3

2.1 Band structure of a solid 6
2.2 Allowed electron transitions 8
2.3 Fermi-Dirac distribution 10
2.4 Photoexcitation 15
2.5 Non-dispersive charge transport 17
2.6 Dispersive charge transport 18
2.7 Two-dimensional crystalline lattice 19
2.8 Crystalline silicon lattice 20
2.9 Atomic and band structures of a two-dimensional amorphous solid 21
2.10 Atomic structure of hydrogenated amorphous silicon 21
2.11 Atomic and band structures of a doped semiconductor 25
2.12 *pn* junction 26
2.13 *pin* solar cell 27

3.1 Multiple-trapping and hopping transport mechanisms 31
3.2 Electron occupation of band tail states after the initial trapping event . . . 35
3.3 Trapping events experienced by a typical electron 37
3.4 Pre-transit electron occupation of band tail states 38
3.5 Electric fields generated by a drifting sheet of charge 40
3.6 High temperature electron occupation of band tail states 43

4.1 Experimental apparatus 48
4.2 Sample mounted on a transistor header 55

5.1 Typical photocurrent trace 58
5.2 Typical current trace plotted on logarithmic scales 59
5.3 Current traces at various temperatures and constant voltage bias 60
5.4 Current traces at constant temperature and various voltage biases 61
5.5 Pre-transit current traces at constant temperature and various voltage biases 62
5.6 Typical photocharge trace 64
5.7 Photogenerated charge at high bias 65
5.8 Photogenerated charge at low bias 66
5.9 Normalized current traces at low temperature 68
5.10 Normalized current traces at high temperature 69
5.11 Normalized charge traces at low temperature 70
5.12 Normalized charge traces at high temperature 72
5.13 Displaceability curves and the mulitple-trapping fit 74

ABSTRACT

Electron transport in an undoped hydrogenated amorphous silicon thin film was studied using the time-of-flight measurement technique. Electrons were injected near the surface of the film with a short laser pulse and pulled through the bulk of the material with an externally applied electric field. The photocurrent resulting from their transit was monitored on an oscilloscope. Current traces were recorded for temperatures between 140 and 200 K and voltage biases between 2 and 8 V. The data are observed to exhibit behavior characteristic of dispersive transport, as is expected for low-temperature electron transport in amorphous materials. A simple multiple-trapping model based on an exponential distribution of thermally activated band tail traps is presented. The model is fit to the collected charge data, obtained by numerical integration of the current traces. The fit is found to be quite good and yields 0.11 $cm^2V^{-1}s^{-1}$ for the microscopic mobility, 1.3×10^{11} s^{-1} for the attempt-to-escape frequency, and 22 meV for the band tail width. These values are comparable to those previously reported, and can be used to describe the transient mobility and displaceability of electrons in the sample.

1

INTRODUCTION

1.1 Motivation

I recently traveled to Senegal, West Africa, where clean water is rare and stable electricity is rarer yet. I was pleasantly surprised to discover that one of the most reliable sources of power—and the only source for rural communities—is photovoltaic devices, or solar cells. After an initial investment to purchase a few solar cells and a battery bank, Senegalese families and businesses enjoy free and clean (though judging by their auto emissions this is not their primary concern) electricity for several decades. Sunlight that would otherwise heat an already hot land is instead used to power lightbulbs, simple appliances, and even a few computers.

Since Russell Ohl [1] accidentally shone a flashlight on a silicon sample at Bell Labs in 1940 and discovered the *pn* junction, solar cells have improved by leaps and bounds. With reduced cost and increased efficiency, new markets have developed so that photovoltaics are now used to power everying from NASA's premier satellites to homes to roadside emergency call boxes. The cells, whose intrinsic material properties allow for photons to be passively and automatically converted into electricity, have come into fame because they capitalize on the abundance of free energy striking Earth each day in the form of sunlight. Of ever increasing importance, solar energy is inexhaustible and completely clean, though there are some emissions associated with the production of solar cells. Photovoltaics will

never be able to escape the role of "supporting power supply" because they depend on weather and location. Nevertheless, they are extremely useful in the right places. With fossil fuel costs permanently on the rise and solar cell technology continually developing, I expect the day is not far off when it will be more economical—not to mention healthier—to look to the sun instead of the Middle East for power.

Historically, photovoltaic research has proceeded by a sort of guess-and-check exploration of semiconducting materials. New materials are developed and then characterized, and changes are made according to the results. In this search the name of the game is maximizing the efficiency-to-cost ratio. Many mechanisms reduce the output of a solar cell including imperfect incident light absorption, recombination of charge carriers, and poor charge transport through the cell [2–6]. In characterizing new materials, these loss mechanisms are studied so that the underlying processes can be understood and the materials improved. This thesis is intended to be a small step in the materials development marathon.

It should be noted that, while I have couched this discussion in the context of photovoltaics, the applications of this thesis are actually farther reaching. The material investigated may also be used for other electronic devices including transistors and flat-panel displays.

1.2 Scope of this thesis

Electron transport is studied in undoped hydrogenated amorphous silicon (a-Si:H) using the time-of-flight (TOF) measurement technique. Amorphous silicon, the younger sibling of the crystalline silicon used in computer chips, is currently a popular photovoltaic material. While not as efficient as its crystalline brethren, it is significantly cheaper and more convenient to manufacture. Undoped a-Si:H comprises the so-called *intrinsic* middle layer of solar cells. It is the thickest layer in the cells and the majority of the electrons' time during transport is spent traversing it. As a result, the electrical properties of the intrinsic layer are a critical factor in determining how well a solar cell will work.

The TOF technique, which was developed in the early 1950's to analyze crystalline

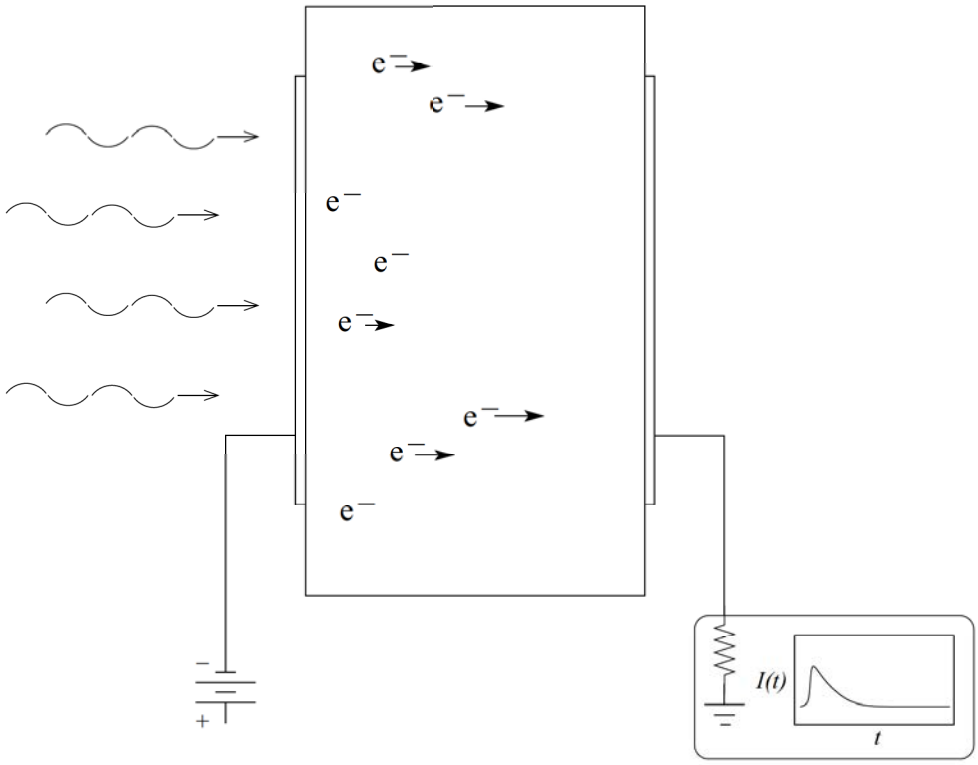

FIGURE 1.1: Time-of-flight measurement technique. A short laser pulse is incident on the sample surface from the left. A voltage bias is simultaneously applied across the width of the sample, causing the photoexcited electrons to traverse the thickness of the sample. The resulting current is recorded on an oscilloscope.

semiconductors during the transistor boom [7–11], investigates charge transport in a material by measuring the current that carriers produce in response to an electric field. The basic idea is described below.

A semiconductor (such as silicon) is made of atoms bonded together in some ordered fashion. In their lowest energy configuration, electrons participate in bonding and their movement is confined. In the TOF experiment, a laser is flashed briefly on a thin semiconducting sample. Some of the electrons near the surface absorb the light's energy, and subsequently they become free to move. A uniform voltage bias is applied across the width of the sample so that the front contact is negatively charged. The photoexcited electrons are repelled from the front contact and begin to traverse the bulk of the sample. In doing so they create a current, which is measured on an oscilloscope (Figure 1.1).

Information about the mobility, or velocity per unit electric field, of the charges can be gleaned from the current they produce. If the electrons travel as a packet with constant

velocity, a steady current will be observed which disappears suddenly when the electrons have traversed the sample. If the electrons slow down or speed up as they cross the sample but continue to move as a coherent group, the current will decrease or increase, respectively, until the electrons complete their transit at which time it will vanish. If the electrons do not move as a packet but instead travel with different velocities and traverse the sample in different times, this also will be reflected in the current, and it will fall off slowly as the charges reach the back contact.

In addition to experimentally measuring how charges move, the TOF technique can provide insight as to why they move as they do. Theories exist which describe possible mechanisms by which electrons interact with the structure of an amorphous material. Each mechanism predicts a particular behavior for electrons subject to an electric field. TOF experiments, which give direct information about electron movement, can thus support or undermine theories about the structure of semiconductors. In this thesis it is found that the multiple-trapping model explains the a-Si:H TOF data well.

2

SEMICONDUCTOR PRIMER

Unfortunately, there are so many variables to consider when discussing solids that generalizations are difficult and exceptions seem to be the rule. What governs the properties of one material may play only a minimal role in a seemingly similar material. I am primarily concerned with introducing important concepts that will be used in later chapters and sometimes I will ignore special cases. Consult Keer [12] for a brief introduction to solid state physics, Ashcroft and Mermin [13] for a more comprehensive and accurate treatment of the subject, Zallen [14] for information about amorphous solids, Street [15] for details about a-Si:H, Böer [16] or Shur [17] for semiconductor device information, and Möller [6] for details regarding photovoltaics.

2.1 Band structure

In a single atom, electrons are allowed to take on only discrete energy, angular momentum, z-component angular momentum, and spin values. These quantities (called *quantum numbers*) uniquely define a *quantum state*, and we say that electrons may occupy only discrete states. According to molecular-orbital theory, bonding between two atoms creates a new set of available states. In a solid with $\sim 10^{23}$ bonded atoms per cubic centimeter, these quantum states are so numerous that they blend together to form quasi-continuous bands of available states separated by inaccessible gaps. This *band structure* is unique to

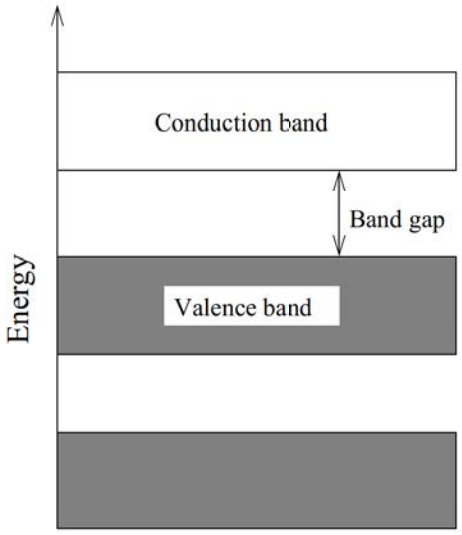

FIGURE 2.1: Band structure of a solid. Note that no information is given on the horizontal axis. The allowed electron energies form bands separated by energy gaps. The uppermost occupied band (occupation is indicated by shading) at absolute zero temperature is identified as the valence band; the band above it is the conduction band. The solid depicted here is either insulating or semiconducting since the valence band is completely filled.

the solid and determines its electronic, magnetic, thermal, and optical properties.

Consider just the energy quantum number. When the available energy states in a solid are plotted, the bands and gaps are seen, as in Figure 2.1. If we were to place electrons one-by-one into a solid, they would naturally move into the lowest available energy states. Since there are a finite number of states available at each energy and the Pauli exclusion priniciple allows only one electron to occupy a given quantum state, the energy bands would fill up as we continued to add electrons. In a solid, the highest energy band that is occupied by electrons at absolute zero temperature is called the *valence band*. The next highest energy band is called the *conduction band*. The energy gap ε_g between these bands is the *band gap*. All the interesting physics happens in the valence and conduction bands, and higher and lower energy bands can be ignored.

2.2 Conductivity

The current density $\vec{J}$ produced in an Ohmic material[1] by an applied electric field $\vec{E}$ is proportional to the field:

$$\vec{J} = \sigma \vec{E}. \tag{2.1}$$

The constant of proportionality σ is known as the electrical conductivity. Solids are grouped in three broad categories based on their conductivities: insulators ($\sigma < 10^{-8}\ \Omega^{-1}\mathrm{m}^{-1}$), semiconductors ($10^{-7}\ \Omega^{-1}\mathrm{m}^{-1} < \sigma < 10^{4}\ \Omega^{-1}\mathrm{m}^{-1}$), and conductors ($\sigma > 10^{5}\ \Omega^{-1}\mathrm{m}^{-1}$). What does the conductivity tell us about a solid? Recalling that

$$\vec{J} = nq\vec{v}, \tag{2.2}$$

where n is the number density of conducting charges, q is their charge, and $\vec{v}$ is their velocity, Eqn (2.1) informs us that in a material with a large conductivity there will be more (or quicker) moving charges for a given electric field than in a small-conductivity material. Apparently then, each charge in a conductor is more mobile than each charge in an insulator, there are more charges moving in a conductor than in an insulator, or some combination of the two.

For a group of charges with zero initial net velocity to conduct a current, they must change states in such a way that they gain a net momentum. In a solid, electrons need nearby unoccupied states (in energy space) for this to occur. Electrons that find themselves surrounded by filled energy states cannot leave their present states; they have nowhere to go. This is shown schematically in Figure 2.2.

Charge transport, or the movement of electrons between free states, happens very differently in conductors and insulators. In metals, electrons can travel within the valence band with little difficulty. As we shall soon see, electron transport in insulators and semiconductors can happen only in the conduction band. In insulators, a formidable energy gap ($\varepsilon_g > 3$ V) keeps electrons from accessing the conduction band, so that charges do not move at all (on average). Semiconductors are simply insulators with band gaps

[1] An Ohmic material is any material that obeys Eqn (2.1).

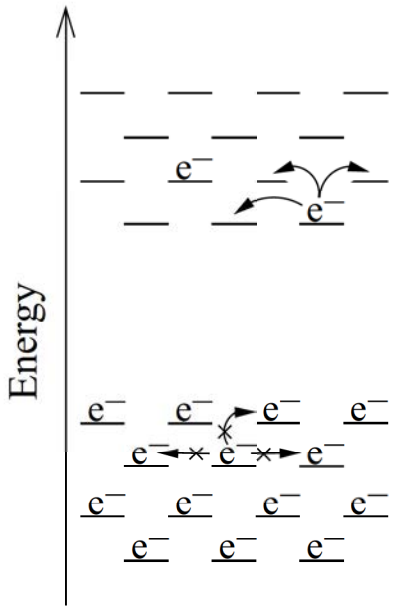

FIGURE 2.2: Allowed electron transitions. Only electrons with empty nearby states can acquire a net velocity. In a semiconductor this occurs in the conduction band.

small enough ($\varepsilon_g < 3$ V) that electrons can sometimes cross the gap and conduct.

For semiconductors, there is an alternative formulation for electrical conductivity that is written in terms of the density of mobile electrons n and the ease with which they move in response to an applied electric field, or *mobility*, μ_n:

$$\sigma = n|e|\mu_n + p|e|\mu_p. \tag{2.3}$$

Here, e is the electronic charge. What, you may ask, is the p term in Eqn (2.3)? I have been slightly misleading thus far: Electron motion is only half the story in conduction. Each electron that is excited into the conduction band leaves behind a *hole* of missing charge where it left the valence band. Another electron in the valence band may move into this hole, creating a new hole in its former location. In this way, holes "move" around the valence band much like the open parking space changes location in the Reed lot on a busy afternoon.[2] As a result it is useful (and customary) to think of holes as positive charge carriers. Thus, p in Eqn (2.3) is the density of free holes and μ_p is the hole mobility.

[2]Do not take this analogy too seriously—to be completely accurate the cars would need to rearrange themselves without leaving the lot.

For now, we will concern ourselves only with pure (or *intrinsic*) crystalline semiconductors for which one mobile hole is generated in the valence band during each electron excitation and hence, $n = p$. With this simplification, Eqn (2.3) reduces to

$$\sigma = n|e|(\mu_n + \mu_p). \tag{2.4}$$

2.3 Charge generation

2.3.1 Thermal excitation

How exactly are electron-hole pairs generated, and how do they affect semiconductor electronic properties? That is, what determines n, and what can it tell us? In the dark, with no externally applied fields, only thermal excitation is possible. In any solid, the probability that a state with energy ε will be occupied with an electron at temperature T is given by the Fermi-Dirac distribution[3]

$$f_n(\varepsilon) = \frac{1}{e^{(\varepsilon-\mu)/kT} + 1}, \tag{2.5}$$

where μ is known as the *chemical potential* (not to be confused with mobility) and k is Boltzmann's constant. The Fermi distribution is shown at several temperature values in Figure 2.3.

The density of occupied states in the energy range ε to $\varepsilon + \mathrm{d}\varepsilon$ is given by the product of the number of states in that range and the probability that each state is occupied. That is,

$$\mathrm{d}n(\varepsilon) = g(\varepsilon) f_n(\varepsilon)\ \mathrm{d}\varepsilon, \tag{2.6}$$

where $g(\varepsilon)$ is the density of energy states (number per unit energy and volume). When Eqn (2.6) is integrated over all energies we must get back the total density of electrons

[3]The Fermi-Dirac distribution gives back the classical Maxwell-Boltzmann distribution at high temperatures.

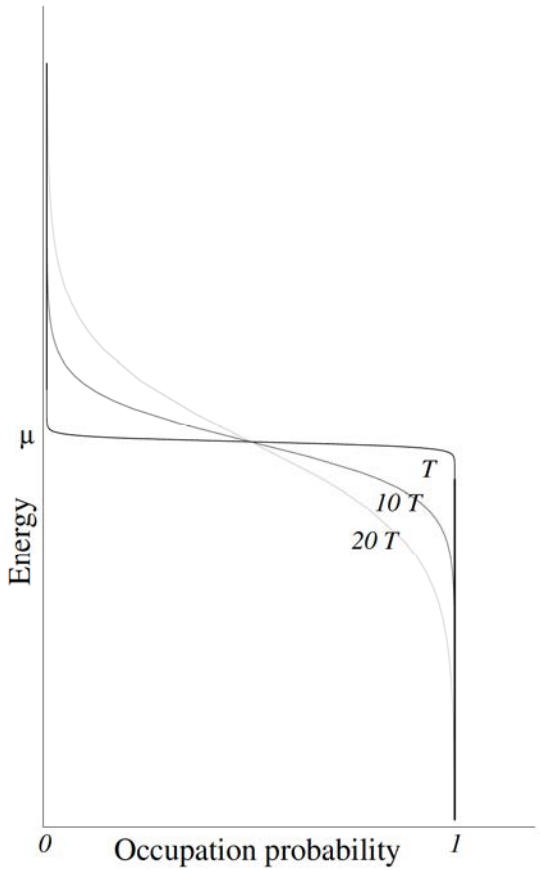

FIGURE 2.3: The Fermi-Dirac distribution. The probability that a state above the chemical potential μ is occupied with an electron is nearly zero at low temperatures, and increases with increasing temperature. One minus the value of the Fermi distribution is the probability that a state is occupied with a hole.

(number per unit volume) in the solid:[4]

$$\begin{aligned}\frac{N}{V} &= \int_0^\infty \mathrm{d}n(\varepsilon) \\ &= \int_0^\infty g(\varepsilon) f_n(\varepsilon)\, \mathrm{d}\varepsilon \\ &= \int_0^\infty \frac{g(\varepsilon)}{e^{(\varepsilon-\mu)/kT}+1}\, \mathrm{d}\varepsilon. \end{aligned} \tag{2.7}$$

Here, and in the rest of the calculations in this chapter, we take the ground state energy to be zero. Equation (2.7) uniquely defines the chemical potential for a given temperature and density of states.

Referring back to Eqn (2.5), notice that as $T \to 0$,

$$f_n(\varepsilon) \to \begin{cases} 0 & \varepsilon > \mu \\ 1 & \varepsilon < \mu \end{cases}$$

and hence, all states below the chemical potential are occupied at absolute zero temperature, while all states above it are empty.[5] If some of the electrons can manage (at non-zero temperatures) to reach states above the chemical potential, they will have a whole sea of empty states to swim in. Thus, μ separates conducting states (for electrons) from non-conducting states, and is an important material parameter. In a metal, the chemical potential lies in the middle of the valence band and electrons immediately below it need very little energy to hop into the conducting states above it. This energy is provided thermally even at low temperatures, causing metals to conduct well.

Where is the chemical potential in an insulator or semiconductor? For intrinsic, crystalline semiconductors it lies in the energy gap. This means that at $T = 0$ every state in the valence band is occupied and every state in the conduction band is empty. As a result, in the valence band the electrons cannot obtain a net velocity (Figure 2.2), and in the conduction band where they are free to move, there are none to move. Unlike in a metal,

[4]Note that I am using lowercase letters for number densities and uppercase letters for numbers.

[5]Many authors are sloppy and use the term *Fermi energy* interchangeably with the chemical potential. The Fermi energy is the energy of the highest occupied state at $T = 0$ and is constant, while the chemical potential is temperature dependent. At $T = 0$ the two quantities take on the same value, and this has given rise to incorrect use of the terms.

a few lattice vibrations will not remedy the situation. In this case, promoting an electron above the chemical potential requires exciting it all the way across the band gap into the empty conduction band. Doing so requires more energy than is thermally available at low temperatures and thus, no conduction occurs.

However, the Fermi distribution tells us that with increasing temperature, it is increasingly likely that states with energy greater than μ (including those in the conduction band) will be occupied.[6] The density of electrons in the conduction band can be calculated from Eqn (2.6) if we know the density of available states:

$$n = \int_{\varepsilon_c}^{\varepsilon_{c\,max}} g(\varepsilon) f_n(\varepsilon)\, \mathrm{d}\varepsilon. \tag{2.8}$$

The limits of the integral are the upper and lower energy bounds of the conduction band. The upper bound may be extended to infinity since at finite temperatures $f_n(\varepsilon)$ drops off sharply above μ, and $g(\varepsilon)$ has no such radical behavior that might compensate. This is important: qualitatively it means that the conducting electrons are concentrated near the conduction band edge, and it justifies our neglect of higher energy bands. Now, for energies several kT above μ the Fermi distribution approximately reduces to the simpler Boltzmann distribution,

$$f_n(\varepsilon) \approx e^{-(\varepsilon-\mu)/kT}. \tag{2.9}$$

Thus, if $\varepsilon_c - \mu \gg kT$, Eqn (2.8) can be written[7]

$$n \approx \int_{\varepsilon_c}^{\infty} g(\varepsilon)\, e^{-(\varepsilon-\mu)/kT}\, \mathrm{d}\varepsilon. \tag{2.10}$$

Finally, it can be shown that the density of states near the conduction band edge[8] has the form $g(\varepsilon) \propto (\varepsilon - \varepsilon_c)^{1/2}$ [18]. With this result, Eqn (2.10) can be easily solved and yields

[6] Of course, even in the high temperature limit it will never be more likely for a high energy state to be occupied than a low energy state.

[7] This is a reasonable assumption for temperatures at or below room temperature. At 300 K, $kT = 0.026$ eV, which is significantly smaller than half the band gap energy in most semiconductors.

[8] The conduction band edge is assumed to be parabolic.

a conduction electron density

$$n \propto (kT)^{3/2}\, e^{-(\varepsilon_c - \mu)/kT}. \tag{2.11}$$

A similar procedure can be used to determine the density of mobile holes in the valence band. If each excited electron leaves a hole in its wake, the probability that a state in the valence band will be occupied by a hole is given by $f_p(\varepsilon) = 1 - f_n(\varepsilon)$ (Figure 2.3). The valence hole density is then

$$p \approx \int_0^{\varepsilon_v} g(\varepsilon)\, [1 - e^{-(\varepsilon - \mu)/kT}]\, \mathrm{d}\varepsilon, \tag{2.12}$$

where $g(\varepsilon)$ is the density of states near the valence band edge ε_v, and the lower limit of the integral has been extended to zero since $f_p(\varepsilon)$ is appreciably large only for states close to the top of the valence band.[9] It has also been assumed that $\mu - \varepsilon_v \gg kT$ so that the Fermi distribution can be replaced by the Boltzmann distribution. As in the conduction band, the density of states near the valence band edge goes as $g(\varepsilon) \propto (\varepsilon_v - \varepsilon)^{1/2}$, and hence,

$$p \propto (kT)^{3/2}\, e^{-(\mu - \varepsilon_v)/kT}. \tag{2.13}$$

Now, recalling that each mobile electron in the conduction band has a corresponding hole in the valence band,

$$\begin{aligned} n &= p \\ &= \sqrt{np} \\ &\propto (kT)^{3/2}\, e^{-(\varepsilon_c - \varepsilon_v)/2kT} \\ &= (kT)^{3/2}\, e^{-\varepsilon_g/2kT}. \end{aligned} \tag{2.14}$$

There are several interesting things to notice here. First, this result is independent of the chemical potential. Second, $(kT)^{3/2}$ varies slowly and the carrier density is dominated by

[9] This implies that hole conduction is concentrated near the valence band edge and lower energy bands can be ignored.

the exponential dependence on temperature. As a result, conductivity in semiconductors increases drastically with increasing temperature. This is contrasted with conductivity in metals, which decreases with heating because mobility is reduced by temperature-dependent scattering and carrier density undergoes no marked increase. Finally, Eqn (2.14) states quantitatively what was previously only conceptually clear: at a given temperature, larger band gaps ε_g correspond to smaller densities of thermally generated carriers (electrons and holes) available for charge transport. This quality is what divides semiconductors and insulators. Semiconductors have small enough band gaps that substantial conductivities are achieved at practical temperatures, and insulators do not.

2.3.2 Photoexcitation

When exposed to light, electrons in semiconductors experience photoexcitation, and this is the foundation of photovoltaics. Suppose monochromatic photons of energy $\varepsilon = h\nu$ are incident on a semiconducting material. If $h\nu < \varepsilon_g$ then the light will not be absorbed by the sample. If, however, $h\nu \geq \varepsilon_g$ then each photon may promote exactly one electron from the valence band to the conduction band (Figure 2.4).[10] In this way, mobile electron-hole pairs are created via absorbed light, and the number of generated carriers is proportional to the light intensity. Electrons that are excited high in the conduction band by very energetic photons quickly fall back down to the conduction edge by interacting with the lattice and releasing the excess energy through lattice vibrations. This thermalization process is usually very short, on the order of a picosecond. This means that, as far as conduction is concerned, the carriers effectively gain only energy ε_g. Blasting a semiconductor with light of energy $h\nu \gg \varepsilon_g$ is no more useful than using light of energy $h\nu = \varepsilon_g$ when trying to create mobile charge carriers. In fact, it is actually detrimental in the case of a-Si:H due to the creation of additional light-induced defects through a phenomenon known as the Staebler-Wronski effect [19].

It is useful to introduce an optical absorption coefficient $\alpha(\lambda)$ defined as the inverse of

[10] Some materials require a simultaneous lattice vibration at the same location that the photon "strikes," even if the photon is sufficiently energetic. See §2.5 for details.

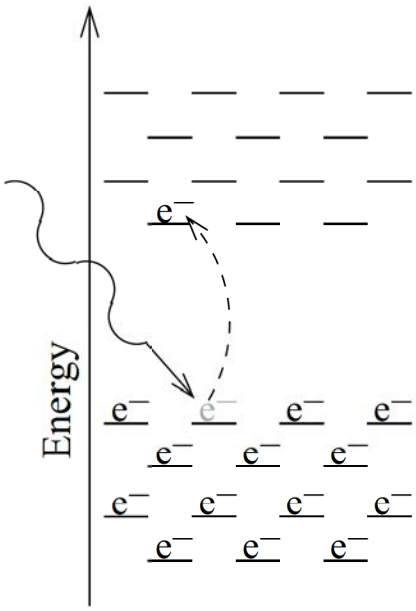

FIGURE 2.4: A sufficiently energetic photon may excite a valence electron into the conduction band, leaving a hole in its wake.

the distance required for the incident (wavelength λ) photon intensity to fall off by a factor of e. This parameter describes how well a material absorbs each wavelength of light and can be used to find the density of electron-hole pairs created per second at each depth from the incident surface. For an illuminated thin-film sample of specified thickness, the larger its absorption coefficient, the better it will conduct. Put another way, to photogenerate a given density of free carriers, more material is required if the absorption coefficient is small.

2.4 Charge transport

In an attempt to understand conductivity in semiconductors we have examined n and p in Eqn (2.3), which has amounted to investigating charge carrier generation. That μ_n and μ_p enter into Eqn (2.3) indicates that we must also be concerned about how free charges *move*. Suppose a packet of electron-hole pairs is created by thermal excitation or photoexcitation. If no electric field is present, the carriers will recombine with one another through one of several recombination methods [4]: radiative recombination, in which an electron in the conduction band emits a photon as it falls into a valence band

hole (opposite of absorption); Auger recombination, in which two free electrons collide, one makes off with all the energy in the form of kinetic energy (it can thermalize back down to the conduction band edge later), and the other joins a hole in the valence band; or recombination through a midgap defect, in which an electron and hole "meet in the middle" by being captured (non-radiatively) by a defect state in the forbidden gap, a process that requires impurities. Of course, an electron does not necessarily recombine with the particular hole with which it was generated; it may end up in a different state than the one it occupied before excitation. When a sample is in thermal equilibrium, the carrier generation rate is balanced by the recombination rate so that carrier concentration remains constant.

If an electric field is present, electrons and holes may be pulled away from one another before they have a chance to recombine. In this case, the carriers move through the sample in opposite directions and generate a current.[11] As shown in Figure 2.5, the current in intrinsic crystals is observed to be constant in time, which indicates that the carriers move with constant velocity. In fact, this is not exactly true. The carriers—which move in their respective band—actually repeatedly accelerate in the electric field and subsequently collide with the lattice (bringing them to a halt). However, this happens on such a short time scale that their velocities appear constant to the macroscopic eye. The *drift mobility* of the carriers is defined as their velocity per unit electric field and can be written[12]

$$\mu_d = \frac{x}{tE}, \tag{2.15}$$

where t is the time it takes a packet of carriers to travel a distance x in a uniform field E. Carrier velocity is proportional to the applied field, making the drift mobility a constant material property. As a result, drift mobility can be determined experimentally by measuring the *transit time* $t = t_\tau$ of carriers moving across a sample of thickness $x = d$, and the result will be independent of the particular d and E chosen. The transit time is well

[11] Note that hole currents and electron currents add rather than canceling each other since the carriers have opposite charge and they travel in opposite directions. This is easy to visualize if we recall that a hole just represents the collective movement of electrons. As a hole moves to the right, what is *really* happening is electrons are jumping (each in the previous electron's spot) to the left.

[12] In general electron and hole drift mobilities are not equal and both must be investigated.

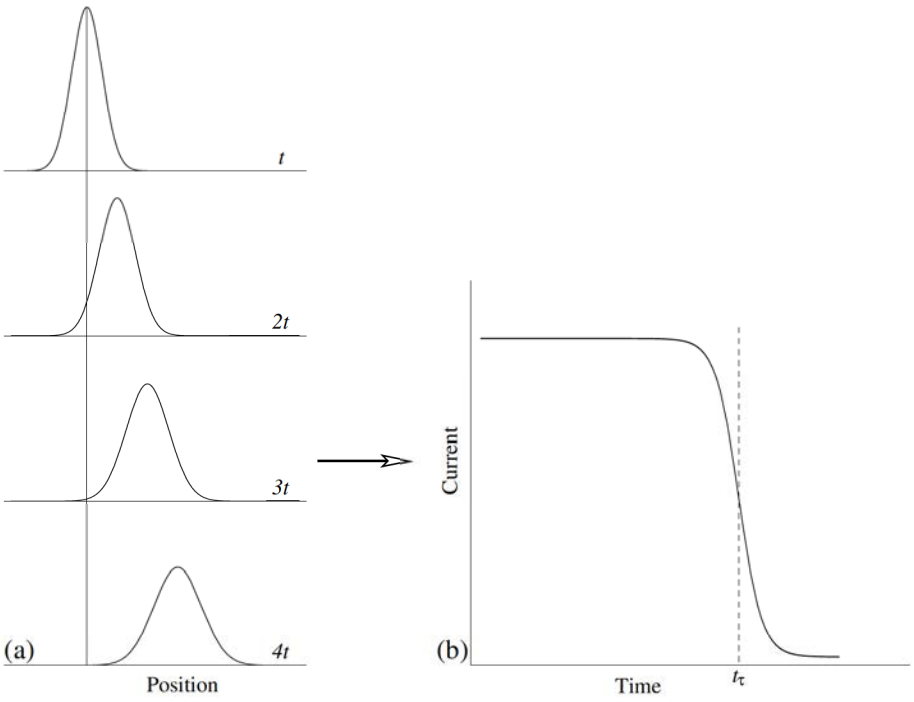

FIGURE 2.5: (a) Time-evolution of a charge packet moving through a crystal in response to an electric field, and (b) the current it produces. The packet moves with constant group velocity and thus generates a constant current. For a sample of finite thickness, the carriers cross the sample at the transit time t_τ and the current drops to zero. There is some non-zero width to the current fall because the carrier packet spreads slightly as it moves.

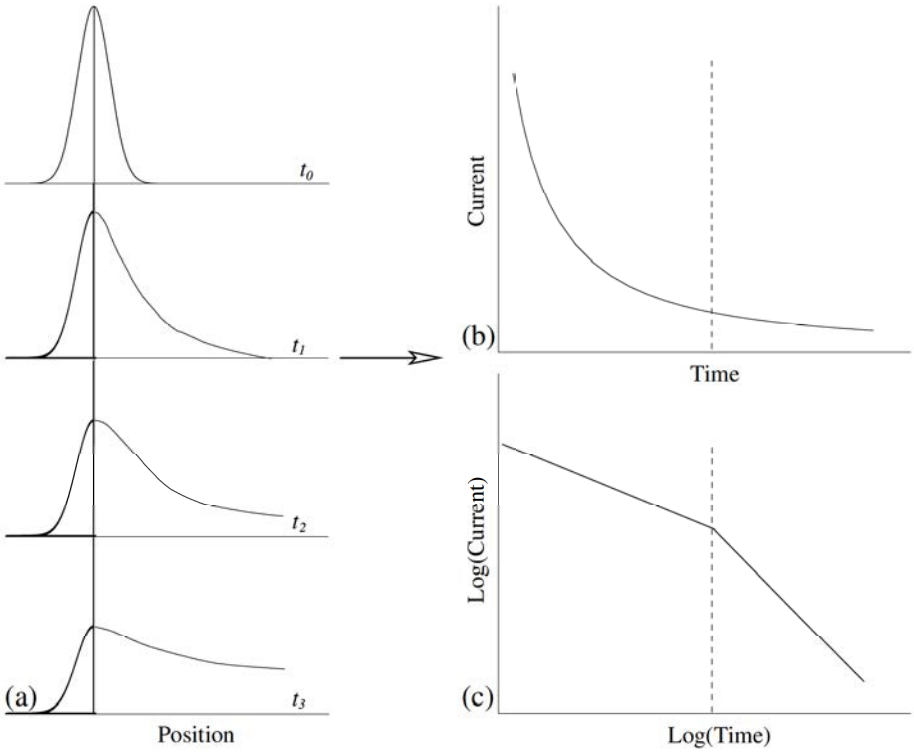

FIGURE 2.6: (a) Time-evolution of a charge packet moving through an amorphous material in response to an electric field, and (b) the current it produces. The peak of the charge packet does not move substantially; instead the packet smears out. Note that the times shown are not necessarily uniformly incremented as in Figure 2.5. The current appears rather featureless, save the immediate and extended decay. However, under a logarithmic transformation (c) it is clear that the current has two distinct regimes, both of which are power law. We call the current prior to the break (indicated with the dashed line) the pre-transit current, and the current after the break the post-transit current.

defined precisely because the carriers move with constant velocity. That is, excepting the usual spreading associated with a moving packet,[13] carriers that begin their travels as a group will arrive at their destination as a group.

Mobility is a tricky quantity in amorphous materials, and a full discussion of the transport theory is saved for Chapter 3. Macroscopically, the current observed when carriers move in an electric field is not constant, indicating that the mobility is time dependent. In particular, the current has two distinct power law regimes, which we call the *pre-transit* and *post-transit* regimes (Figure 2.6). Transport that exhibits these characteristics is said to be *dispersive*. Dispersive transport corresponds to a packet of carriers that spreads out

[13]This spreading is known as diffusion in transport studies. Dispersion, the standard term, is reserved for another sort of transport.

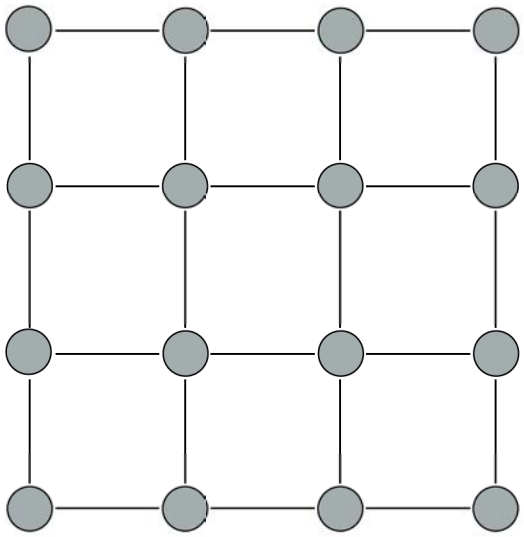

FIGURE 2.7: Two-dimensional crystalline lattice. Atoms are represented by filled circles and bonds are drawn as lines between atoms. Notice the structural periodicity that defines crystalline materials.

in time and loses its shape, due to a wide range of carrier velocities. Carriers do not share a common transit time like they do in crystals, and it is unclear what time should be used in Eqn (2.15). As a result, mobilities are best determined using alternative methods. The analysis techniques are saved for Chapter 5.

2.5 Crystalline vs. amorphous

Until now, this primer has been primarily concerned with a single, specific, and ideal type of semiconductor: the intrinsic crystal. Variations on the physics described are observed when the crystal structure is perturbed even slightly, since perturbations change the bonding scheme that gives rise to the energy bands. This inflexibility accounts for the huge number of interesting and very different semiconductor materials, and is both a blessing and a curse. A discussion of impurities is saved for §2.6; structural variations of intrinsic materials are discussed below.

In a crystal, atoms are arranged in a periodic array which minimizes their total energy. An illustrative two-dimensional crystal structure, or *lattice*, is shown in Figure 2.7. We say that crystals exhibit long-range order, by which we mean that a wandering electron will see the exact same structure repeated as it translates through the solid.

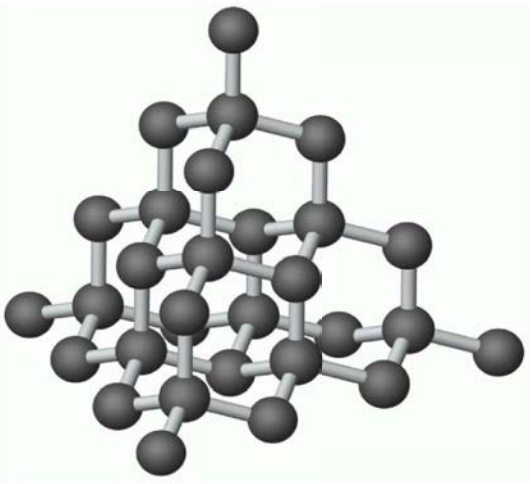

FIGURE 2.8: Crystalline silicon lattice [20]. Each atom has four-fold coordination since silicon has four valence electrons, and the atoms are arranged in the diamond structure.

In the case of crystalline silicon, shown in Figure 2.8, each silicon atom has four valence electrons and thus wants to bond with four other atoms. The number of nearest neighbors to which an atom is bonded is called its *coordination*, so each silicon atom is satisfied with a coordination of four. The lowest total energy configuration for the material is achieved when each silicon atom is tetrahedrally bonded, forming the so-called diamond structure.

How does an amorphous material differ from a crystalline material? Suppose that a solid is heated up and then quenched, or cooled very quickly. In this process, atoms do not have time to find their ideal lattice sites before they are frozen in place, and disorder is introduced into the structure. Like a bumped chess game, atoms are slightly and randomly misplaced, and the periodic crystalline structure is lost. There still exists some idea of the ideal orientation and the atoms are approximating that fictional arrangement, but they all approximate it in a different way. Materials with these properties are called *amorphous* (Figure 2.9) and are said to have short-range or local order, but lack long-range order. A wandering electron will pick up on the overall pattern but will also notice anomalies in the landscape.

Most of the disorder in amorphous materials is due to bent bonds. We might imagine that bonds are also stretched or compressed; however, stretching requires significantly more energy than bending and is not observed. Coordination defects or *dangling bonds* also occur, meaning that an atom is left with one fewer neighbor than it would like. In

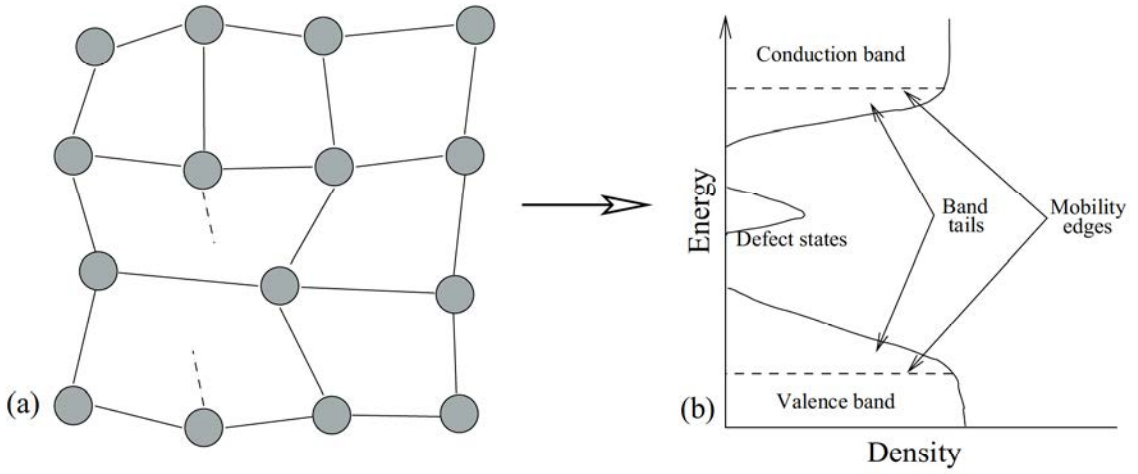

FIGURE 2.9: (a) Atomic structure of a two-dimensional amorphous solid, and (b) the associated band structure. Bent bonds and coordination defects give rise to localized band tail states. A mobility edge separates these states from the extended band states.

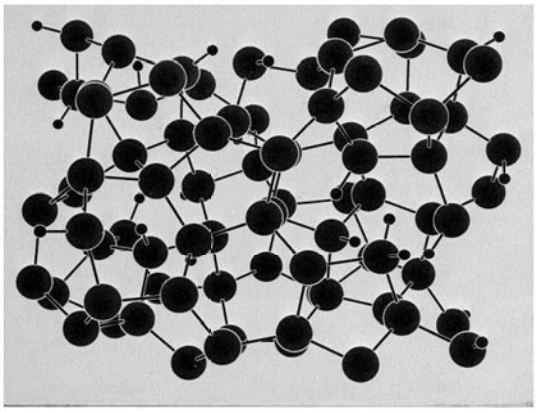

FIGURE 2.10: Atomic structure of hydrogenated amorphous silicon [21]. Bent bonds and coordination defects passivated with hydrogen (shown here as small spheres) destort the silicon structure from its crystalline form.

terms of band structure, these structural perturbations blur the edges of the conduction and valence bands by creating *band tails* that extend a short distance (in energy space) into the gap.[14] It is no longer clear where the bands begin and end, and the terms *mobility gap* and *mobility edge* are introduced in place of "band gap" and "band edge."

The atomic structure of amorphous silicon is shown in Figure 2.10. Because of bent bonds, the material lacks the crystalline structure seen in Figure 2.8. Dangling bonds are also present; in this case they are passivated by hydrogen introduced in the growth process

[14]Recall from §2.1 that the accessible quantum states are determined by bonding, and thus altering the bonds alters the states.

(hence the "hydrogenated" in a-Si:H).

The long-range order in crystals corresponds to a periodic potential, which leads to solutions of the Schrödinger equation that are extended in space.[15] With an increasingly disordered potential, the coherence of the wavefunction decreases and it becomes increasingly localized in space. Anderson [23] demonstrated that with enough disorder, the wavefunction will be entirely localized and electrons will be bound. In amorphous materials, the lack of long-range order means that the band tail states are localized. Electrons are unable to move in band tail states, and the states have rightfully earned the name *traps*.[16] The mobility edge just introduced is the energy that separates the extended conduction or valence band states from their localized band tails, if such a distinct cut-off exists. Naturally, the mobility gap is the energy gap between the valence and conduction mobility edges.

Although the density of band tail states is small, they play an important role in charge transport because conduction occurs at the mobility edges where they are located. In crystalline materials, the only prerequisite for carrier transport is that the carriers have available energy states to move into. In amorphous materials this is not enough, since traps also impede transit, regardless of whether or not the surrounding states are occupied. Electrons moving in the conduction band may fall into the lower energy traps and be temporarily (or not!) deterred. This reduces the average mobility of the carriers.

Why then, if carriers are less mobile in amorphous materials, is a-Si:H used in photovoltaics? Although the reduced carrier mobility decreases solar cell efficiency, there is an unseen advantage to a-Si:H solar cells. Because the wavefunction in a crystal is spatially periodic, the Hamiltonian operator commutes with the momentum operator, and hence, momentum is conserved. In some materials (known as *direct gap* semiconductors), the conduction band minimum aligns with the valence band maximum in momentum space so that momentum conservation comes for free in electron-hole pair generation. In other

[15] These are known as the Bloch solutions and have the form $\psi(x+a) = e^{(iKa)}\psi(x)$ where a is the "wavelength" of the periodic potential and K is some constant [22].

[16] There is nothing fundamentally different about traps and other defect sites in the gap that act as recombination centers. However, recombination does not occur at band tail states because the states are near the mobility edge and hence, the thermal release time of trapped carriers to the band is much shorter than the recombination time.

materials (called *indirect gap* semiconductors), however, the bands' extrema are separated not only by an energy gap, but also by a momentum gap. This means that an electron must be given both sufficient energy and momentum to be excited to the conduction band. Usually photons can give the necessary energy only,[17] and a simultaneous lattice vibration or *phonon* is needed to impart momentum. Because of the unlikelihood of this event, indirect gap materials tend to have small optical absorption coefficients and, in the case of photovoltaics, thick cells are required to absorb most of the incident light. Thicker cells cost more money to manufacture, and this hurts the sought after efficiency-to-cost ratio.[18]

This problem may be skirted by preparing indirect gap materials in their amorphous form. By shaking up the lattice a bit and throwing away long-range order, momentum conservation is also lost. Electron-hole pair generation can then be accomplished by photons alone, and absorption coefficients increase dramatically. Much less amorphous material is needed to absorb most incident sunlight, and thin-film photovoltaics are becoming a reality. For example, a-Si:H requires only one-twentieth the distance needed by crystalline Si to absorb the same amount of light [4]. Thus, although introducing disorder in semiconductors compromises carrier mobility, it can also reduce cost.

2.6 Doping

Though not immediately relevant to the experimental work in this thesis, let us briefly investigate doping and junctions so that we can understand the physics of an amorphous solar cell and get a better grasp on the motivation for this research.

An *impurity* is an atom that occupies a lattice site where an atom of a different element should be. Impurities pervade every material in some concentration, and they are the pure-semiconductor-grower's worst nightmare. However, when introduced on purpose and in a controllable fashion (known as *doping*), a whole new collection of extremely useful materials is born.

If a semiconductor is doped with an element with one more valence electron than the

[17] $\varepsilon = pc$ and since c is large, p must be small to give photon-like values of ε.

[18] At this point, it may seem practical to just forget about indirect gap crystals and concentrate on direct gap materials for photovoltaic devices. However, many of the most abundant (and therefore cheapest) semiconducting materials on Earth have indirect gaps, including Si and Ge.

intrinsic element, then the dopant atoms will want one less bond than the surrounding host atoms. When forced to form one more bond than they would prefer, the dopant atoms (called *donors*) will have one loosely bound valence electron left over (Figure 2.11).[19] Semiconductors that are doped in this fashion are called negative- or n-type. On the other hand, if the dopant atoms (called *acceptors*) have one fewer valence electron than the host atoms, there will be an extra hole that does not participate in bonding. Semiconductors that are doped in this fashion are called positive- or p-type. Note that n-type semiconductors are not overall negatively charged and p-type semiconductors are not overall positively charged. Both are neutral, but have an excess of either free electrons or free holes.

With the introduction of impurities comes new energy states in the band (or mobility) gap called *defect states*. Unlike band tail states, defect states do not blend into the conduction and valence bands. Though distinct, the defect states lie closer to the conduction band than the valence band in an n-type semiconductor. Some of these states are occupied with electrons at absolute zero temperature because donor atoms have provided extra non-bonding electrons, and this shifts the chemical potential towards the conduction band. Conversely, defect states in a p-type semiconductor are near the valence band, and excess holes provided by acceptor atoms shift the chemical potential towards the valence band.

2.7 Junctions

Suppose a p-type semiconductor is laid on top of an n-type semiconductor to form a pn junction. As shown in Figure 2.12, there will be a difference in the chemical potentials of the materials due to the addition of dopants. As a result, the loosely bound donor electrons in the n-type material will flow into the p-type material to lower their energy. There, they will recombine with excess holes to form negative ions. Similarly, holes will diffuse from the p-type material into the n-type material and form positive ions. This separation of carriers means that the n-type material becomes positively charged near

[19] In a-Si:H, the dopant atoms are ionized for $T > 100$ K and the extra electron is not bound at all.

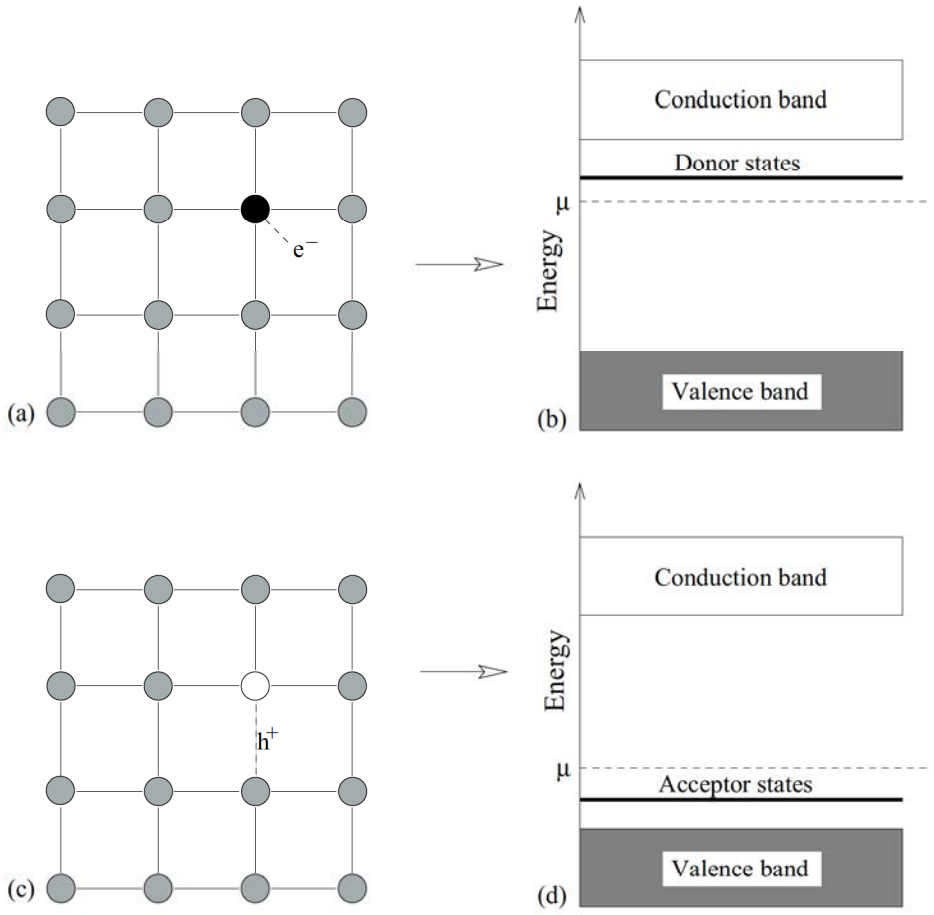

FIGURE 2.11: (a) Atomic structure of an n-type semiconductor and (b) the associated band structure. Donor atoms each have one extra valence electron left after bonding, and the presence of these electrons shifts the chemical potential upwards. (c) Atomic structure of an p-type semiconductor and (d) the associated band structure. Acceptor atoms each have one extra hole (or one too few valence electrons) left after bonding, and the presence of these holes shifts the chemical potential downwards.

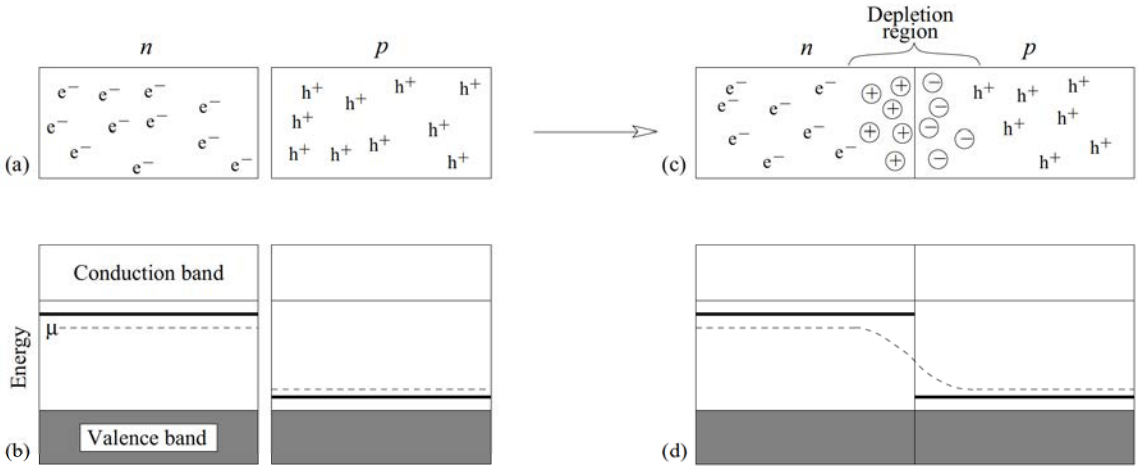

FIGURE 2.12: (a) An n-type semiconductor has an excess of free electrons (indicated as e^-) and a p-type semiconductor has an excess of free holes (indicated as h^+) that (b) shift the chemical potentials away from mid-gap. When these materials are brought in contact, (c) charges diffuse across the pn junction and create a depletion region. Here positive ions are indicated as $\oplus$ and negative ions are indicated as $\ominus$. (d) The chemical potential bends in the depletion region so that it is single valued at the junction.

the junction and the p-type material becomes negatively charged. The charged region, which is of finite extent since the electrostatic force limits charge separation (equilibrium is reached), is known as the *depletion region*. The depletion region acts as a built-in voltage potential, and injected carriers have a preferential direction of travel.

A *pin* structure is used in a-Si:H photovoltaics,[20] where the i- or intrinsic-layer is undoped and significantly thicker than the p- and n-layers (Figure 2.13). A depletion region is present at both junctions and a built-in voltage potential is established. Incoming light passes through the thin p-layer and is absorbed in the i-layer, producing electron-hole pairs. The internal electric field separates the charges and pulls them towards the appropriate contacts. They flow through an external circuit, and—voilá!—electricity.

Carriers spend most of their time traversing the thick i-layer in a functioning solar cell, and the way in which they move through it critically affects the cell's output. Are all of the photogenerated carriers collected at a contact? Do they experience recombination? How much time do carriers spend in traps? Do the traps slow carriers down so much that there is a build up of charge that screens the internal field and limits the current output?

[20] pn junctions are used for crystalline silicon solar cell, but the defect density in n- and p-type a-Si:H is too high for efficient electron-hole pair photogeneration. An i-layer in which electron-hole pairs are more easily produced is added to combat this.

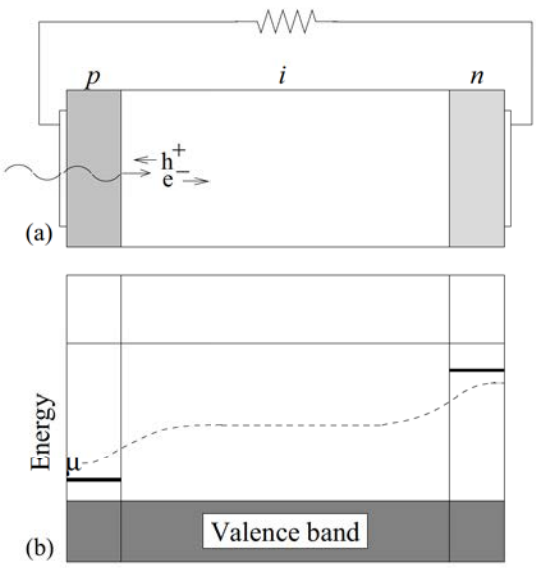

FIGURE 2.13: Photovoltaic device with *pin* structure. (a) Photogenerated carriers are separated by (b) the built-in potential caused by the *n*- and *p*-type layers, and they travel around the circuit through the load.

Clearly, in order to understand the solar cell, we must first understand charge transport in a-Si:H.

3

THEORY

3.1 Overview

Carrier transport in amorphous materials is not entirely understood. Several simple models have bounced around the scientific community in the last thirty years;[1] however, the underlying physics of materials with aperiodic structure is exceedingly complex, and no single theory fits all the data perfectly. The most widely accepted model for transport at reasonable temperatures is the *multiple-trapping model*. In this theory, transport is limited by the emission rate of thermally activated band tail traps. Mobile carriers in the bands tend to fall into these lower energy traps where they become (temporarily or not) immobilized. They must wait to be thermally reemitted to the band before they can participate in transport again. Most carriers undergo multiple trapping events, and this is where the theory derives its name.

Development of the multiple-trapping model began in 1975 when Scher and Montroll [28] reported that the power law current decay observed in dispersive transport (Figure 2.6) can be described mathematically by a broad distribution of "event times" given by the function:

$$\psi(t) \propto t^{-\alpha-1}, \tag{3.1}$$

where α is a number between 0 and 1 that is related to the disorder in the material.

[1] For a good review see Marshall [24], Orenstein et al. [25], Pfister and Scher [26], or Tiedje [27].

Scher and Montroll arrived at this result by developing a continuous time random walk (CTRW) theory in which carriers drift randomly, but have a preference for movement in a particular direction.[2] In this model, $\psi(t)\mathrm{d}t$ is the probability that a carrier at a particular site (location in space) will arrive at the next site between times t and $t+\mathrm{d}t$. The disorder in amorphous materials means that sites are non-identical, and hence there is a broad distribution in the movement times between adjacent sites. Despite its remarkable success in uncovering the mathematics behind dispersive transport, the CTRW theory offered no physical transport mechanism.

In 1977, Noolandi [29] and Shmidlin [30] independently showed that $\psi(t)$ can be derived from the rate equations that describe the multiple-trapping mechanism. That is, Scher and Montroll's mathematics fall out if the event times are release times from immobilizing traps. Three years later, Orenstein and Kastner [31] and Tiedje and Rose [32] presented the first conceptual pictures of multiple-trapping, and both developed simple, approximate expressions describing dispersive transport based on qualitative arguments. The following discussion follows the work of these last authors. Only electrons will be discussed, although the same arguments can be applied trivially to valence band hole transport.

It should be noted that multiple trapping is only one possible transport mechanism. Carriers may also undergo phonon-assisted tunneling between traps of similar energy, without ever being released to extended band states (Figure 3.1). This mechanism is known as *hopping*. At most temperatures hopping is a small effect and does not contribute significantly to transport. However, at very low temperatures ($T < 50$ K for electrons and $T < 200$ K for holes in aSi:H [15]) trapped electrons do not have enough energy to escape to the conduction band and hopping actually becomes the dominant mechanism.

3.2 Assumptions

Consider a sample of thickness d under the conditions specified by the idealized TOF experiment (Figure 1.1).[3] A sheet of electron-hole pairs is generated near the front surface

[2] In TOF-type experiments for which the model was developed, the preferential direction is due to an applied electric field, and the degree of preference reflects the magnitude of the field.

[3] Details are reserved for Chapter 4.

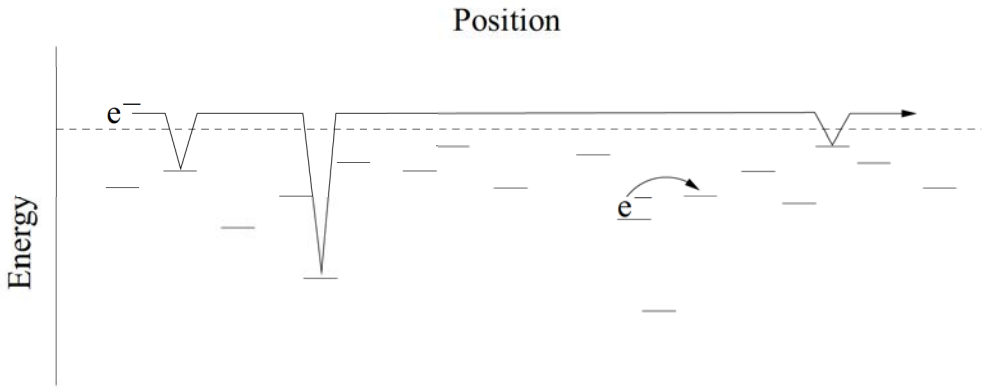

FIGURE 3.1: Multiple-trapping and hopping transport mechanisms. The electron on the upper left translates in space in the conduction band. Its movement is periodically interrupted by trapping in band tail states (multiple trapping). The other electron tunnels directly between localized states (hopping).

by a uniform optical excitation pulse at $t = 0$. A constant voltage bias is applied across the sample. The holes are swept to the front contact and out of the sample quickly in response to the electric field, and the electrons drift for a much longer period of time through the bulk of the material. In doing so, they generate a field of their own (assumed to be small compared to the applied field) and induce a current $I(t)$ (I call it the *photocurrent*) that flows from the conductive back contact. We will consider transport only for $t < 1$ ms, after which recombination sets in. In this time regime, no carriers are permanently lost and thus, according to Eqns (2.1) and (2.3), a decrease in current reflects a decrease in carrier mobility.

There are three assumptions made in the multiple-trapping model. First, it is assumed that there is a distinct mobility edge that separates localized states from extended states. Carriers in the extended states may move and possess mobility (called the *microscopic mobility*) μ_0, while carriers in the localized states are immobile. Transport, then, occurs only above the mobility edge. This assumption is based on work by Abrahams et al. [33] that predicted that a sharp mobility edge in three-dimensional amorphous materials is a consequence of Anderson localization.

Second, the band tail density of states is assumed to fall off exponentially away from

the mobility edge:

$$g(\varepsilon) = g_0 \, e^{-\varepsilon/kT_c}, \qquad \varepsilon > 0 \tag{3.2}$$

where g_0 is the density of states at the mobility edge and T_c is a temperature such that $\Delta\varepsilon = kT_c$ is the energy from the mobility edge at which the density of states has dropped to g_0/e (i.e., $\Delta\varepsilon$ characterizes the band tail width). For convenience during calculations, throughout this chapter ε is taken to be zero at the mobilty edge with positive energy pointing into the gap. The trap distribution is assumed to be fixed so that $g(\varepsilon)$ is not affected by the experimental conditions. Recent work by Aljishi et al. [34] suggests that this is not necessarily the case and that in a-Si:H $\Delta\varepsilon$ depends linearly on temperature for $T > 350$ K. Luckily, we are primarily interested in temperatures that are lower than this, for which the band tail width was found be to constant.

The assumed exponential tail shape was also predicted by Abrahams et al. [33] (in three-dimensions only), and countless papers [31, 35–41] have found that it explains the data well. Intuitively, it is not clear how much deviation from this shape will still account for the data, and several authors have explored alternative distributions. For example, Marshall et al. [42] and Nebel and Bauer [43] found that a density of states that is linear near the mobility edge and exponential at deeper trap energies fits the data at least as well as a purely exponential distribution.

Above the mobility edge, we assume that the density of states is both constant and continuous with the trap distribution at the edge so that

$$g(\varepsilon) = g_0. \qquad \varepsilon \leq 0 \tag{3.3}$$

Finally, it is assumed that all traps have equal probability of capturing an electron, regardless of the trap energy. That is, an electron is equally likely to fall into a particular trap at the top of the band tail as it is to fall into a particular deep trap. Stated technically, we say the traps have constant *capture cross section*. We understand this to mean that the distance from a localized state inside of which a wandering electron will "fall in" is

the same for all band tail states, independent of their depth. This need not be the case, and in fact some authors [44] have included an energy-dependent capture cross section. However, it is well established from experimental data that capture is much faster than release, making release the rate-determining step in transport. Introducing a variable cross section is therefore superfluous; in terms of the total time spent between trapping events, it makes negligible difference whether an electron moving through an amorphous material interacted with some traps that took 10^{-10} s to capture it, and others that only took 10^{-14} s.

Given constant capture cross section, detailed balance (presented in Appendix A) leads to the conclusion that the average release time from a trap at energy ε is

$$t_r(\varepsilon) = \frac{1}{\nu}\, e^{\,\varepsilon/kT}, \tag{3.4}$$

where ν is an *attempt-to-escape frequency* that describes how often a trapped carrier tries to escape. Thus, capture is an energy-independent process, but release is not.

3.3 Recovering $\psi(t)$

Functional inversion of Eqn (3.4) gives the energy associated with each release time:

$$\varepsilon(t_r) = kT\, \ln(\nu t_r). \tag{3.5}$$

The release time distribution discovered by Scher and Montroll, $\psi(t)$, can now be recovered. $\psi(t)\mathrm{d}t$ is simply the fraction of states with release times between t and $t+\mathrm{d}t$:[4]

$$\begin{aligned}\psi(t)\mathrm{d}t &= \frac{\mathrm{d}m(t)}{\int \mathrm{d}m} \\ &= \frac{g(t)\mathrm{d}t}{\int g(\varepsilon)\mathrm{d}\varepsilon} \\ &= \frac{g(\varepsilon)\,\frac{\mathrm{d}\varepsilon}{\mathrm{d}t}\mathrm{d}t}{\int g(\varepsilon)\mathrm{d}\varepsilon}.\end{aligned}$$

[4] I use m here so that n can be reserved for electron densities.

Using Eqns (3.2) and (3.5),

$$
\begin{aligned}
\Rightarrow \psi(t) &= \frac{g(\varepsilon)}{\int g(\varepsilon)\mathrm{d}\varepsilon}\,\frac{\mathrm{d}\varepsilon}{\mathrm{d}t} \\
&= \frac{g_0\, e^{-\varepsilon/kT_c}}{g_0 \int_0^\infty e^{-\varepsilon/kT_c}\,\mathrm{d}\varepsilon}\,\frac{\mathrm{d}}{\mathrm{d}t}[kT\,\ln(\nu t)] \\
&= \frac{e^{-\varepsilon/kT_c}}{kT_c}\,\frac{\nu kT}{\nu t} \\
&= \frac{e^{-[kT\,\ln(\nu t)]/kT_c}}{kT_c}\,\frac{\nu kT}{\nu t} \\
&= \frac{\left[e^{\ln(\nu t)}\right]^{-T/T_c}}{T_c}\,\frac{\nu T}{\nu t} \\
&= \frac{\alpha\nu(\nu t)^{-T/T_c}}{\nu t} \\
&= \alpha\nu(\nu t)^{-\frac{T}{T_c}-1}. \qquad (3.6)
\end{aligned}
$$

The multiple-trapping model looks promising; Eqn (3.6) has the same form as Eqn (3.1) with $\alpha = T/T_c$. This is important: we have imbued the previously lifeless parameter α with physical meaning. Scher and Montroll [28] found that $0 < \alpha < 1$ for dispersive transport. Apparently, multiple trapping predicts dispersive transport for $T < T_c$.

3.4 Short times

According to the multiple-trapping model, the pre-transit photocurrent observed in TOF experiments on amorphous materials decays because carriers are increasingly immobilized in traps. Given the assumptions in §3.2, we can quantify this process and derive the observed power law form of the pre-transit current (Figure 2.6).

3.4.1 Electron occupation

Immediately after photoexcitation, electrons may be broadly dispersed energetically in the conduction band, depending on the energy of the incident light. However, Vardenay and Tauc [45] showed that within 10^{-12} s the electrons *thermalize* down to the bottom of the conduction band and into the band tail states. Thermalization refers to the interaction between carriers and phonons by which the carriers move to lower energy states. Since the

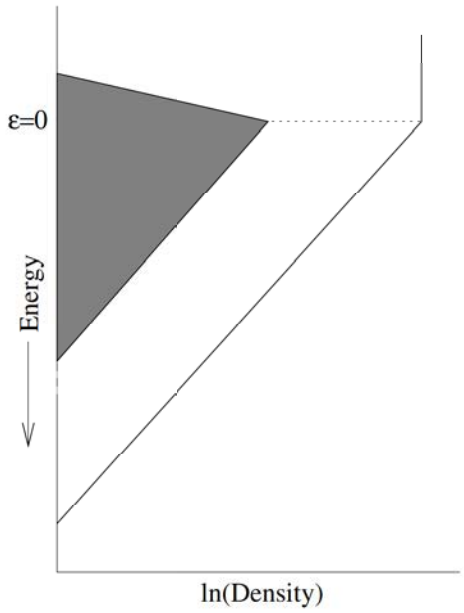

FIGURE 3.2: Electron occupation of band tail states after the initial trapping event. The conduction band and band tail are shown, and the mobility edge which separates them is indicated with the dashed line. Occupation (shaded states are occupied) parallels the density of states in the band tail because of the constant capture cross section assumption. Notice that in this figure and those that follow, the logarithm of the density of states is plotted on the horizontal axis, and we take $\varepsilon = 0$ to be at the mobility edge, with positive energy pointing into the band gap.

energy released in these transitions is carried off by phonons and the energy of a phonon is related to its frequency, the thermalization rate is on the order of a phonon frequency (10^{12} s^{-1}) [15].

Following the initial trapping event, electron occupancy parallels the density of states in the band tail (Figure 3.2). This occurs because, according to the constant capture cross section assumption, the density of carriers trapped at each energy is proportional to the density of states. We assume that there are not so many photogenerated carriers that the trap levels become saturated; this would lead to non-dispersive transport and would likely disturb the uniformity of the applied electric field. Furthermore, we assume that once initially trapped, the electrons must be released to the conduction band before they may move. That is, they must undergo mulitple trapping. Hopping is neglected because its effects are negligible in the temperature range studied in this thesis.[5]

[5]Note that occupation diagrams such as Figure 3.2 are deceptive in that hopping looks like the most favorable transport mechanism. However, we have to remember that these diagrams give an average

Returning to Eqn (3.5), we can understand how carriers interact with the band tail after the first trapping event if we introduce a time-dependent demarcation energy $\varepsilon^*(t)$, such that the release time from traps at $\varepsilon^*(t)$ is equal to the time that has passed since the carriers were initially generated:

$$\varepsilon^*(t) = kT \ln(\nu t). \tag{3.7}$$

Obviously, the rate at which $\varepsilon^*(t)$ makes its way down the band tail decreases with increasing time. At any particular time, traps below $\varepsilon^*(t)$ have not emitted electrons,[6] since by definition these traps have an average release time greater than the time that has passed. Hence, electron occupation below $\varepsilon^*(t)$ remains parallel to the density of states. That is, the density of electrons between ε and $\varepsilon + d\varepsilon$ is

$$\begin{aligned} dn(\varepsilon) &= F(t)g(\varepsilon) \\ &= F(t)g_0\, e^{-\varepsilon/kT_c}, \qquad\qquad \varepsilon \geq \varepsilon^*(t) \end{aligned} \tag{3.8}$$

where $F(t)$ is a proportionality constant that indicates what fraction of the states at $\varepsilon^*(t)$ are occupied at time t.

States above $\varepsilon^*(t)$, on the other hand, have emitted trapped electrons at least once, and most have emitted many times. Each time an electron experiences reemission, it has equal chance to be trapped by any of the unoccupied band tail states. If it falls into a shallow state it will be reemitted quickly; if it falls into a deeper state it will be trapped longer. Since shallow states emit more often than deep states but collect at the same rate, electrons tend to accumulate in deeper states. This process is shown for one representative electron in Figure 3.3.

Like any particles that have many opportunities to sample states, the electrons above

picture of what is going on in the sample and they do not show spatial information. In fact, states of similar energy (between which hopping naively looks good) may not be anywhere near each other in space.

[6] I mean below $\varepsilon^*(t)$ on occupation diagrams like Figure 3.4, which actually corresponds to larger energies than $\varepsilon^*(t)$ because of our coordinate choice.

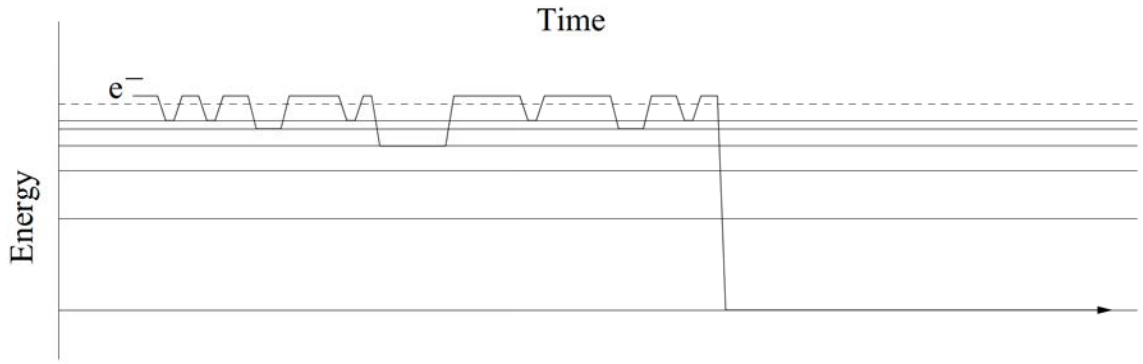

FIGURE 3.3: Trapping events experienced by a typical electron. The electron falls into shallow states often and is released quickly. The deeper it is trapped, the longer it must wait for thermal reemission. Eventually it is trapped in a very deep state since it has equal probability of falling into any single state, and it is stuck for a long time.

$\varepsilon^*(t)$ thermalize and form a Boltzmann distribution centered at $\varepsilon^*(t)$. Mathematically,

$$dn(\varepsilon) = F(t)g(\varepsilon)\, e^{\,[\varepsilon-\varepsilon^*(t)]/kT}\, \mathrm{d}\varepsilon. \qquad \varepsilon \leq \varepsilon^*(t)$$

This breaks into two cases according to the density of states. In the conduction band,

$$dn(\varepsilon) = F(t)g_0\, e^{\,[\varepsilon-\varepsilon^*(t)]/kT}\, \mathrm{d}\varepsilon. \qquad \varepsilon \leq 0 \tag{3.9}$$

Between the conduction mobility edge and demarcation energy,

$$\begin{aligned} dn(\varepsilon) &= F(t)g_0\, e^{\,-\varepsilon/kT_c}\, e^{\,[\varepsilon-\varepsilon^*(t)]/kT}\, \mathrm{d}\varepsilon \\ &= F(t)g_0\, e^{\,-\varepsilon^*(t)/kT}\, e^{\,\varepsilon(\frac{1}{kT}-\frac{1}{kT_c})}\, \mathrm{d}\varepsilon \\ &= F(t)g_0\, e^{\,-\varepsilon^*(t)/kT}\, e^{\,\frac{\varepsilon}{kT}(1-\alpha)}\, \mathrm{d}\varepsilon. \qquad 0 \leq \varepsilon \leq \varepsilon^*(t) \end{aligned} \tag{3.10}$$

Here $F(t)$ is included so that Eqns (3.8) and (3.10) give the same result at $\varepsilon^*(t)$. For $\alpha = T/T_c < 1$, Eqn (3.10) tells us that electron occupation decreases exponentially from the demarcation energy towards the mobility edge. In this case, electron occupancy in the tail states is strongly peaked at $\varepsilon^*(t)$ (Figure 3.4). It falls off exponentially below $\varepsilon^*(t)$ due to the decrease in the density of states, and above $\varepsilon^*(t)$ because of the Boltzmann distribution. As $\varepsilon^*(t)$ moves through the band tail in time, the peak electron density does

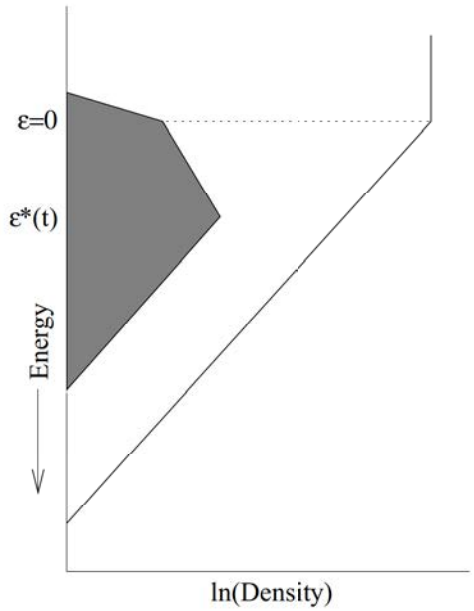

FIGURE 3.4: Pre-transit electron occupation of band tail states at low temperatures ($T < T_c$). Occupation decreases due to thermalization above $\varepsilon^*(t)$, and the density of states distribution below $\varepsilon^*(t)$.

so as well, probing the tail states one energy at a time.

3.4.2 Transient mobility

The high concentration of electrons at $\varepsilon^*(t)$ suggests that we treat the system as having only a single trap level. For a single immobilizing trap level, the average mobility of all the carriers at a particular time is the microscopic mobility μ_0 reduced by the fraction of carriers that are trapped:

$$\mu(t) = \mu_0 \frac{n_{free}}{n_{free} + n_{trapped}}. \tag{3.11}$$

Many authors call this quantity the drift mobility ($\mu(t) = \mu_d$). This is a terrible practice since the drift mobility obtained from the TOF-determined transit time (Eqn (2.15)) is the average mobility of the carriers averaged over all the time that has passed since the start of the experiment. Schiff et al. [46, 47] call $\mu(t)$ the transient drift mobility to indicate its time dependence. I prefer to call it the *transient mobility* to avoid any confusion with μ_d. Note that Eqn (3.11) implicitly assumes that the microscopic mobility is a temperature-independent material parameter and that the temperature dependence of the transient

mobility is completely determined by the fraction of trapped carriers.

Assuming the number of trapped carriers is much greater than the number of free carriers, or equivalently, $\mu(t) \ll \mu_0$, then

$$\mu(t) \approx \mu_0 \frac{n_{free}}{n_{trapped}}. \tag{3.12}$$

Based on previous arguments, we make the approximation that all of the trapped carriers are within $d\varepsilon$ of $\varepsilon^*(t)$. Furthermore, and for the same reasons, we make the approximation that all the free carriers are at the mobility edge. From Eqns (3.8) and (3.9),

$$\begin{aligned}
\mu(t) &\approx \mu_0 \frac{dn(0)}{dn(\varepsilon^*)} \\
&= \mu_0 \frac{F(t)g(0)\ e^{(0-\varepsilon^*)/kT}\ d\varepsilon}{F(t)g_0\ e^{-\varepsilon^*/kT_c}\ d\varepsilon} \\
&= \mu_0 \frac{g_0\ e^{-\varepsilon^*/kT}}{g_0\ e^{-\varepsilon^*/kT_c}} \\
&= \mu_0\ e^{\varepsilon^*(\frac{1}{kT_c}-\frac{1}{kT})} \\
&= \mu_0\ e^{-\frac{\varepsilon^*}{kT}(1-\alpha)}.
\end{aligned}$$

Inserting the demarcation energy from Eqn (3.7),

$$\begin{aligned}
\mu(t) &\approx \mu_0\ e^{-\frac{kT\ln(\nu t)}{kT}(1-\alpha)} \\
&= \mu_0\ \left[e^{\ln(\nu t)}\right]^{-(1-\alpha)} \\
&= \mu_0\ (\nu t)^{\alpha-1}.
\end{aligned} \tag{3.13}$$

This approximate result differs by only a factor of $\sin(\alpha\pi)/(\alpha\pi)$ from the rigorous results obtained by Schmidlin [30] and Orenstein et al. [25]. Note that $\mu(t)$ carries temperature dependence hidden in α.

3.4.3 Photocurrent

As the electrons drift, they perturb the electric field in the sample slightly, and the charges on the conductive contacts must rearrange in order to keep the electric potential V across

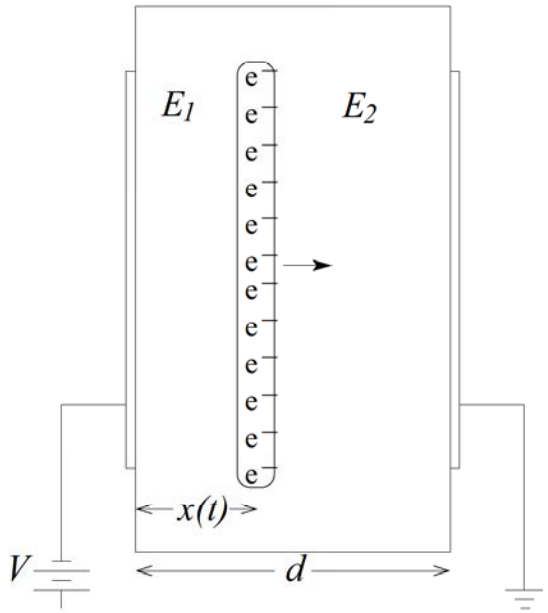

FIGURE 3.5: Schematic of a sheet of charge drifting in a sample in response to a constant voltage bias. The sheet, which has been substituted in place of a more complex spatial distribution, alters the electric field in the sample as it moves. The changing fields cause a displacement current to leave the conductive back contact.

the sample constant (V is what we actually set on our instrument). Conveniently, before any carriers complete their transit, the dispersed spatial distribution of electrons moving at different speeds creates the same redistribution of charge on the back contact as a narrow sheet of electrons that maintains its shape and moves with speed $v = \mu(t)E$ (Figure 3.5), where E is the applied electric field. The position of this "equivalent effect" sheet is

$$x(t) = \int_0^t \mu(t)E \, \mathrm{d}t. \tag{3.14}$$

$x(t)/E$ is called the *displaceability* and indicates how far the average carrier subject to the field E moves in time t.

If E_1 is the electric field behind the drifting sheet and E_2 is the field in front of it, then

$$\begin{aligned} V &= \int_0^d \vec{E} \cdot \mathrm{d}\vec{l} \\ &= E_1 x(t) + E_2[d - x(t)]. \end{aligned} \tag{3.15}$$

From Gauss' Law applied to the drifting sheet,

$$\int \vec{E} \cdot \mathrm{d}\vec{a} = \frac{Q_{encl}}{\epsilon}$$
$$\Rightarrow A(E_2 - E_1) = \frac{Ne}{\epsilon}, \tag{3.16}$$

where N is the total number of photoexcited electrons, A is the area in which they were generated, and ϵ is the dielectric constant of the material. Equations (3.15) and (3.16) can be solved easily and give

$$E_1 = \frac{V}{d} - \frac{Ne}{\epsilon A}[1 - \frac{x(t)}{d}] \tag{3.17}$$
$$E_2 = \frac{V}{d} + \frac{Ne}{\epsilon A}\frac{x(t)}{d}. \tag{3.18}$$

Finally, from the generalized form of Ampere's Law, the displacement current that leaves the back contact prior to the arrival of any carriers is

$$\begin{aligned} I(t) &= \epsilon A \frac{\mathrm{d}E_2}{\mathrm{d}t} \\ &= \frac{Ne}{d}\frac{\mathrm{d}x(t)}{\mathrm{d}t} \\ &= \frac{Ne}{d}\mu(t)E \qquad (3.19) \\ &= \frac{\mu_0 ENe}{d}(\nu t)^{\alpha-1}. \qquad (3.20) \end{aligned}$$

This has the power law decay characteristic of the pre-transit regime of dispersive transport (Figure 2.6).

3.5 Long times

The pre-transit current decays because electrons accumulate in deep traps, but what accounts for the sharp break seen in Figure 2.6? In other words, how can we explain the post-transit current?

As $\varepsilon^*(t)$ marches down the band tail in time, it becomes less and less likely that carriers in the conduction band will be trapped at energies below it, since the density of states

decreases exponentially. At some time, for now we will call it the *first carrier arrival time* (t_{1st}), there are so few unoccupied states below $\varepsilon^*(t_{1st})$ that a carrier emitted to the conduction band is more likely to complete its transit (through the usual multiple trapping in shallow states) than be trapped below $\varepsilon^*(t_{1st})$. Hence, after t_{1st} no new electrons are trapped below $\varepsilon^*(t_{1st})$. In this long-time regime, the photocurrent is limited by the emission times of occupied deep traps rather than the trapping of electrons. In particular, it can be shown [27, 32, 36] that:

$$I(t) \propto t^{-\alpha-1}. \tag{3.21}$$

As expected, the post-transit current has power law behavior and decreases more quickly than the pre-transit current. Equations (3.20) and (3.21) predict that, for a TOF current trace plotted on logarithmic axes, the pre- and post-transit currents will appear as straight lines with slopes $\alpha - 1$ and $-\alpha - 1$, respectively. Thus, adding the slopes should yield -2. This provides a nice way to check the multiple-trapping theory.[7]

Macroscopically, the current break at t_{1st} is due to the finite thickness of the sample. As the name implies, the post-transit current decreases because carriers complete their transit. The transient mobility does not change at t_{1st}; there are simply fewer carriers in the sample contributing to the current. As a result, the post-transit current does not yield any information about the carriers' interactions with the band tail or their movement through the material.

3.6 High temperatures

For $T > T_c \Rightarrow \alpha > 1$, Eqn (3.10) indicates that electron occupancy *increases* exponentially from $\varepsilon^*(t)$ to the mobility edge.[8] In this case, the trapped electron density is peaked at the mobility edge and not at $\varepsilon^*(t)$ (Figure 3.6).

As a result, $n_{trapped} \gg n_{free}$ no longer holds, and Eqn (3.12) is an invalid approxima-

[7] However, in practice it is not always observed that the sum of the pre- and post-transit current slopes is -2. In some cases the post-transit current has power law form, but cannot be described by Eqn 3.21 with $0 < \alpha < 1$.

[8] For electrons in a-Si:H, $T_c \approx 300$ K—well above the temperatures explored in this thesis.

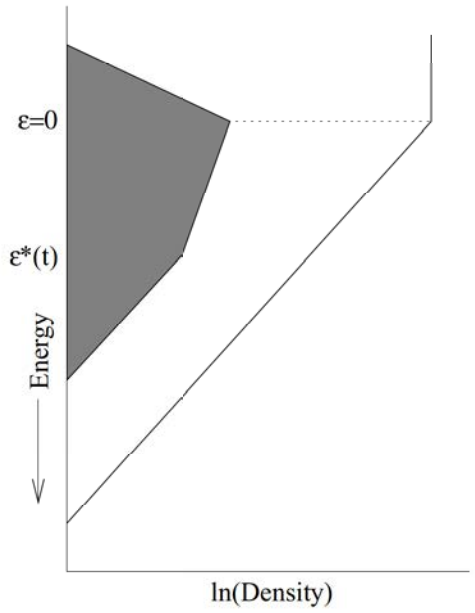

FIGURE 3.6: High temperature electron occupation of band tail states. For $T > T_c$, photoexcited electrons are concentrated at the mobility edge instead of the demarcation energy, and transport becomes non-dispersive.

tion. Working instead straight from Eqn (3.11), Tiedje et al. [48] showed that

$$\mu(t) \approx \mu_0 \frac{\alpha - 1}{\alpha}. \qquad \alpha > 1 \tag{3.22}$$

The high temperature mobility (and hence the current) has no time dependence, indicating that transport is non-dispersive. Qualitatively, at high temperatures the release times from the traps are so short that trapping has little effect on transport, and the carriers are able to maintain their sheet-like shape. In this limit, amorphous transport mimics crystalline transport, although carrier mobilities are significantly lower. For very high temperatures Eqn (3.22) predicts $\mu(t) \approx \mu_0$, and it is tempting to think that the microscopic mobility can be determined trivially by high temperature TOF measurements. However, such experiments do not necessarily measure what they intend to; as mentioned, Aljishi et al. reported that the microscopic mobility is not constant at high temperatures.

3.7 Transit time

In most of the literature dealing with dispersive transport, extensive reference is made to the *transit time* and *drift mobility*. This section is dedicated to sorting out the many definitions used for these terms, as well as convincing you that they should be used with care when describing dispersive transport.

The drift mobility μ_d and transit time t_τ were introduced in Eqn (2.15) as obeying the following relationship in *crystalline* materials:

$$\mu_d = \frac{d}{Et_\tau}. \tag{2.15}$$

Typically, t_τ is measured experimentally and subsequently, μ_d is determined with this expression. Physically, t_τ is the time it takes a sheet of carriers to cross the crystal, and μ_d is their average velocity per unit electric field averaged over t_τ:

$$\mu_d = \frac{1}{t_\tau}\int_0^{t_\tau} \mu(t)\,\mathrm{d}t. \tag{3.23}$$

Of course, for non-dispersive transport the carriers travel with constant velocity and thus,

$$\mu_d = \mu(t). \tag{3.24}$$

Many authors have tried to retain the use of Eqn (2.15) for dispersive transport, but doing so is dangerous. The transit time must be arbitrarily defined since the spread of the carriers is enormous and the carriers do not complete their transit simultaneously. Each carrier has its own transit time, and a sensible definition might be the average of these individual times. However, some electrons are trapped for the entire duration of the experiment and never reach the back contact so that

$$t_\tau = \sum_{i=1}^{N} t_{\tau_i} \tag{3.25}$$

is infinite.

A more useful approach is to arbitrarily associate t_τ with some recognizable feature on photocurrent traces.[9] The most obvious choice is the break in the power law current decay, i.e., $t_\tau = t_{1st}$. Experimentally, the transit time is found by fitting two power law functions to pre- and post-transit regimes, and identifying their intersection. The drift mobility is then found from Eqn (2.15).

Unfortunately, it is observed that the drift mobility depends (non-linearly) on the sample thickness and applied electric field. What does the multiple-trapping model have to say about this? It is commonly argued [48,49] that a reasonable physical interpretation of the transit time is the time at which the average carrier has traversed half the sample. Mathematically,

$$\int_0^{t_\tau} \mu(t) E \, \mathrm{d}t = \frac{d}{2}. \tag{3.26}$$

With the insertion of $\mu(t)$ from Eqn (3.13),

$$\begin{aligned} \frac{d}{2} &= \mu_0 E \int_0^{t_\tau} (\nu t)^{\alpha-1} \, \mathrm{d}t \\ &= \mu_0 E \, \frac{(\nu t_\tau)^\alpha}{\alpha\nu} \\ \Rightarrow t_\tau &= \frac{1}{\nu} \left(\frac{\alpha\nu}{2\mu_0} \right)^{\frac{1}{\alpha}} \left(\frac{d}{E} \right)^{\frac{1}{\alpha}}. \end{aligned} \tag{3.27}$$

Notice that with this physical interpretation, the transit time has non-linear sample thickness and electric field dependence. Using this result in Eqn (2.15),

$$\mu_d = \nu \left(\frac{\alpha\nu}{2\mu_0} \right)^{-\frac{1}{\alpha}} \left(\frac{d}{E} \right)^{1-\frac{1}{\alpha}}. \tag{3.28}$$

As is found experimentally, the drift mobility has strange field and thickness dependence. This is an artifact that arises from the transit time. The drift mobility is inherently time dependent[10] (Eqn (3.23)), and evaluating it at different transit times picks up the transit

[9] Note that now the transit time is not defined in relation to some physical event, such as the completed transit of the photoexcited carriers. Instead, it is just a name for a point shared by photocurrent plots. Although it will soon become clear that finding mobilities from the transit time is not a fruitful approach in amorphous materials, I will continue to use the term to identify the current break observed in dispersive transport.

[10] This can be confusing. The drift mobility is actually a function of time, but it is always evaluated at a particular time (namely the transit time) and is thus always used as a number in the literature.

time's field and thickness dependence. This makes it very difficult to compare transport in different samples, since it is only legitimate to compare results that were recorded with the same ratio of d/E. The drift mobility as obtained from Eqn (2.15) is thus a poor parameter for characterizing transport in amorphous materials; better techniques exist and will be used in Chapter 5.

4

EXPERIMENTAL METHODS

4.1 Overview

All measurements in this thesis were performed with a TOF apparatus I constructed. TOF experiments measure the current produced when photogenerated carriers traverse a semiconducting sample in the presence of an externally applied electric field. The transient mobility of the carriers can be determined directly from the results, and important electronic parameters such as the microscopic mobility, attempt-to-escape frequency, and band tail width can be obtained by fitting the data to the predictions of the multiple-trapping model. Mobility measurement techniques like TOF are especially useful for examining low mobility samples for which the common Hall technique yields results that are difficult to interpret. TOF is perhaps the simplest of a few such mobility measurements because it separates electron transport from hole transport so each can be studied independently. It also has drawbacks, and the limitations of the experiment will be discussed throughout this chapter. For a comprehensive description of the TOF technique, refer to Spear [50].

The TOF apparatus used is shown in Figure 4.1. A short laser pulse triggered by a pulse generator was incident on the front surface of a thin-film sample. The wavelength of the light was chosen such that the photons were absorbed very close to the front surface, creating a sheet of mobile electron-hole pairs. Shortly before the laser pulse, a constant voltage bias was applied across the thickness of the sample. Under the influence of the

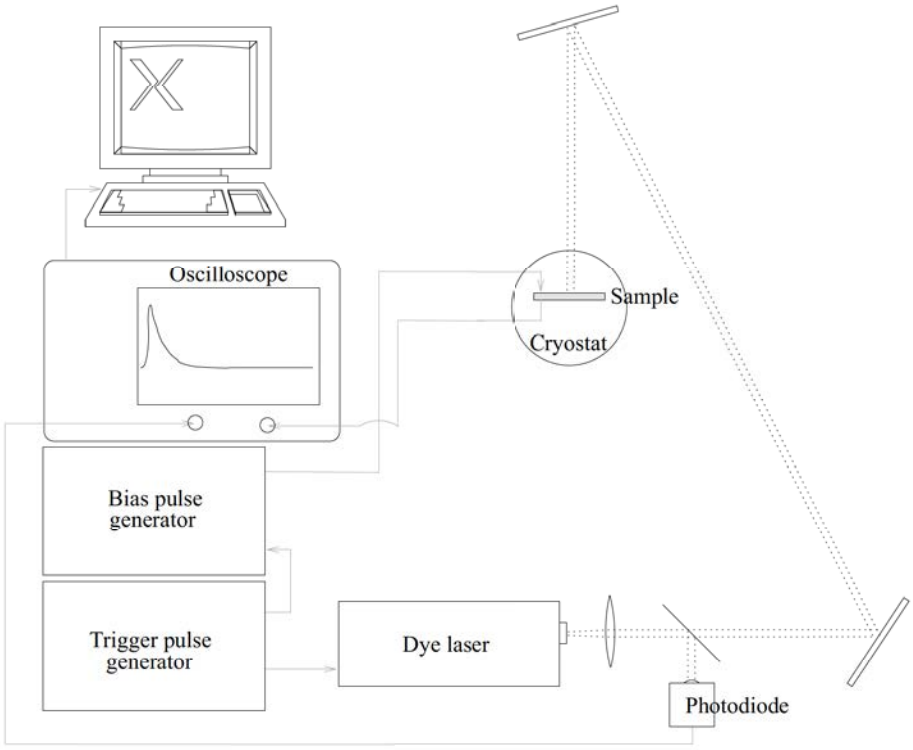

FIGURE 4.1: Experimental apparatus. Laser pulses illuminated a sample in a cryostat, as well as triggered an oscilloscope. The carriers generated in the sample by the light were separated by an applied electric field according to their charge. The holes completed their transit very quickly; the electrons had to traverse the bulk of the sample. The current produced during their movement was recorded on the oscilloscope and imported into a computer.

bias, the photogenerated carriers were separated according to their charge. In particular, a negative voltage was applied to the front contact, and the holes traveled a very short distance to this contact while the electrons were repelled into the bulk of the material. The movement of the electrons caused a displacement current to leave the *Ohmic* back contact.[1] The front contact was *blocking* so that the carriers that were swept out the back were not replaced.[2] The current from the back contact was recorded on a digital oscilloscope that was triggered by a photodiode. A beamsplitter sent a fraction of the light to the photodiode each time the laser flashed, so that the scope began taking data when the light struck the sample.

4.2 Equipment

Details on the proper instrument parameters for a-Si:H TOF were found primarily in papers by Schiff et al. [37, 51, 52] and Tiedje et al. [27, 35, 36].

4.2.1 Laser

A Laser Science (now Spectra Physics) VSL-337 tunable dye laser provided illumination. The nitrogen plasma cartridge in the laser emitted ultraviolet pulses of laser light that pumped a cuvette filled with dye. By selecting the proper dye and adjusting a diffraction grating, any frequency of visible light could be obtained. I used Coumarin 460 dye (available from Exciton, Inc.) and selected a wavelength of 458 nm. The absorption coefficient of a-Si:H at this wavelength is $\alpha = 3.21 \times 10^5$ cm^{-1} [53], indicating that two-thirds of the incident photons were absorbed within the first two percent of the sample thickness from the front surface. It is desirable that the light be absorbed near the front surface since the holes will complete their transit very quickly and the observed photocurrent can be attributed solely to electrons traversing the bulk.

The laser was externally triggered using a Hewlett Packard 8112A pulse generator so that the bias could be synchronized with the laser pulses. The 8112A delivered 3 μs wide, 5 volt TTL pulses, according to the triggering requirements of the laser. The repetition

[1] An Ohmic contact allows charge to pass freely through it in either direction.
[2] A blocking contact, or *Shottky barrier*, allows charge to pass through in only one direction.

rate was set to 1 Hz so that the bias was off long enough between pulses for the charges in the sample to return to equilibrium. The dimensions of the laser beam were roughly 3 mm $\times$ 8 mm. Each pulse of laser light was 3 ns long and carried roughly 100 μJ of energy. This incredibly short pulse length is ideal for TOF experiments, since we require that the pulse length be much shorter than the transit time in order to approximate the initial carrier distribution as a sheet in space. With a long laser pulse (relative to t_τ), interpreting photocurrent data would be similar to trying to determine who won a foot race from finish-line times alone, when the runners did not share a common starting point.

The dye laser emitted radio-frequency noise during each gas discharge, which unfortunately was picked up by the ocsilloscope. The signal was large enough to mask the current trace recorded from the sample for approximately 500 ns after each pulse, so that measurements at very short times were infeasible. Experiments indicated that the radio-frequency noise propagated through the air and not down cables or wires, so that isolating the laser electronically did nothing to fix the problem. Although the intensity of the noise decreased as the laser was moved away from the other electronics, the scope was able to trigger on the signal even with a wall between it and the laser. No simple solution for eliminating the noise was found; instead I limited my measurements to longer times ($t > 500$ ns). A new Spectra Physics dye laser was recently purchased and initial tests suggested that it may not have the same problem.

4.2.2 Optics

The laser beam was focused on a beamsplitter which reflected five percent of the light onto a photodiode and transmitted the rest. The photodiode, a Newport biased detector with a rise time of less than 350 ps, triggered the oscilloscope so that the scope began taking data coincident with the laser pulse. The light that was transmitted through the beamsplitter reflected off two adjustable mirrors and hit the sample inside the cryostat. With the adjustable mirrors and a camera focused on the sample, aligning the beam on the sample was easy as pie.

4.2.3 Bias voltage

A pulsed voltage bias was applied to the front contact of the sample by a Hewlett Packard 8111A pulse generator. The 8111A was triggered by the 8112A instrument 17 μs before the laser was triggered so that the bias began approximately 20 μs before the laser flash was incident on the surface.[3] Applying the bias prior to the arrival of the laser beam swept out any carriers in the sample that may have been mobile due to thermal excitation. This ensured that the current recorded during the experiment was due to photogenerated carriers alone.

For those authors who determine mobility from the transit time, it is necessary that the voltage bias be applied long enough that the current break is observed. This was of no concern to us since we determined mobility directly from the pre-transit photocurrent. However, there was an upper limit on the bias time. At long times ($t > 1$ ms), photoexcited electrons recombine with holes at defect states and are no longer available for transport.[4] Furthermore, midgap defect states emit electrons that screen the applied electric field after the so-called *dielectric relaxation time*. In addition to disturbing the uniformity of the field, the movement of these non-photogenerated carriers shows up on current traces. In light of these concerns, the width of the bias pulse was maintained at 250 μs.

When applied, the bias was kept constant. Values from -2 V to -8 V were used; all were negative so that electron (and not hole) transport was investigated. This range was used for two reasons. First, if the bias is too small, the applied field will not be significantly larger than the field generated by the drifting carriers. In order to assume that the field in the sample is constant, the photogenerated charge Q_0 must be negligible compared to the charge $Q = CV$ applied to the contacts (C is the sample capacitance).[5] Schiff et al. [37] found that this was violated for $V \leq 1$ V in a sample of similar thickness

[3] There was a 3 μs delay between the trigger time and firing time of the laser.

[4] We want to associate changes in the observed current with changes in carrier mobility, so we ensured that current-affecting parameters (such as a reduction in the number of carriers or non-constant electric fields) were controlled.

[5] It is not inconsistent to assume that the field created by the drifting carriers induces a measurable current and yet is negligible compared to the applied field. The generalized form of Ampere's Law says that only changes in the electric field produce a displacement current, and the applied field is constant. Hence, changes in the overall electric field in the sample are detectable even if they are tiny compared to the constant applied field.

to the sample in the present study. Second, fields that are too large will cause dielectric breakdown in the sample.

4.2.4 Oscilloscope

A Tektronix TDS 744A digitizing oscilloscope connected to the back contact of the sample recorded the current generated by the photocarriers. An input resistance of 50 Ω—much smaller than the impedance of the sample—was chosen so that essentially all of the applied voltage was dropped across the sample and not across the oscilloscope's internal resistor. With this setup, the photocurrent in amps was one-fiftieth the voltage drop measured across the resistor during the experiment.

The oscilloscope was run in single acquisition mode, which means that it began taking data when it received a trigger signal, and stopped after a set length of time (between 2.5 μs and 20 μs). The photodiode response provided the trigger, so that the oscilloscope was synchronized with the pulsing laser. The input resistance on the trigger channel was set to 50 Ω in order to match the impedance of the BNC cable. This prevented electrical signals from reflecting at the cable-scope junction and producing an unreliable trigger signal. Five thousand data points were recorded during each acquisition. The oscilloscope took one data set each time the laser pulsed and averaged the individual signals. One hundred acquisitions were averaged in each experiment.

4.2.5 Computer

A LabVIEW TDS 744A driver (available from www.ni.com) was used to query the oscilloscope and receive the data after each experiment. Slight modifications were made to the driver so that the data were saved to the hard drive. Microsoft Excel was used to manage and plot the data.

4.2.6 Temperature control

Samples were mounted inside a custom-made quartz cryostat. Dry nitrogen gas passed through a copper tube immersed in a liquid nitrogen-filled dewar, and then entered the

cryostat. The cold nitrogen gas cooled the sample and also provided the water-free environment necessary for electrical measurements. The gas flow was controlled with a flow meter, allowing sample temperatures below 100 K to be achieved at high flow levels. The cryostat was vacuum jacketed for thermal insulation, and a roughing pump kept the pressure at 10^{-2} Torr.

For higher temperatures, a Nichrome heater in the cryostat warmed the incoming nitrogen. A platinum resistance thermometer mounted next to the sample recorded the sample temperature, and a LakeShore DRC-93C digital controller on which the desired temperature was set adjusted the heater power accordingly. This setup was both accurate and stable—during experiments the sample temperature was held constant to within 0.1 K.

The ability to vary the temperature between experiments is important because dispersive transport is controlled by traps with temperature-dependent release times. In particular, we want to know if the experimentally observed temperature dependence of the mobility agrees with that predicted by Eqn (3.13). As discussed in §3.1 and 3.6, transport at very low temperatures becomes hopping-limited, and transport at high temperatures becomes non-dispersive. Thus, sample temperatures of 140-200 K were used in all experiments.

4.3 Samples

David Cohen of the University of Oregon generously donated seven amorphous silicon samples for TOF examination. The samples had an $(s.s.)n^{+}i$ structure, where $s.s.$ was a stainless steel substrate, and n^{+} was a thin (40-50 nm) layer of a-Si:H doped with a high concentration of phosphine.[6] The n^{+}-layer served to form an Ohmic junction between the intrinsic layer and the conductive stainless steel substrate. Because of the high concentration of donors, a very narrow depletion region was formed in the n^{+}-layer and carriers tunneled through it easily in either direction. The i-layers were germanium-alloyed hydrogenated amorphous silicon (a-Si_xGe_{1-x}:H), and each sample had a different

[6]The + indicates that the layer was highly doped, not that it was charged.

concentration of germanium. Each i-layer was roughly 2 μm thick and was deposited via hot wire chemical vapor deposition of silane. Semitransparent palladium dots 1 mm in diameter were evaporated on the front surface of each sample to form Schottky barrier contacts.

For electrical measurements, these samples are effectively modeled as a parallel resistor and capacitor. If the resistor impedance is small compared to the capacitor impedance, the sample is said to be leaky and will effectively act Ohmic. In leaky samples, a current will be observed in TOF experiments whenever the bias is applied, regardless of whether the laser hit the sample. Thus, the capacitor impedance must be small relative to the resistor impedance in order to analyze transport through the i-layer.

Simple capacitance measurements were used to check if the samples leaked. A 10 kIIz AC signal was applied to each sample, and a lock-in amplifier compared the samples' responses to the input signal. Analysis of the equivalent circuit reveals that the in-phase component of each sample's response is related to the inverse of the resistance, and the out-of-phase component is related to the capacitance. A large in-phase component (relative to the out-of-phase component) implies that the sample is leaky. Surprisingly, all the samples were found to leak save the sample with no germanium alloying. For this sample, comparison of the out-of-phase signal to that of a capacitor with known capacitance yielded an equivalent circuit capacitance of 58 pF.

The i-layer of the unalloyed a-Si:H sample was deposited at a rate of 1.62 Å/s for an estimated thickness of 1.75 μm. The thickness can also be estimated from the sample capacitance: $d = k\epsilon_0 A/C$, where $k = 11.7$ is the dielectric constant of silicon, $\epsilon_0 = 8.85 \times 10^{-12}$ Fm^{-1} is the permativity of free space, and $A = \pi(2.5 \times 10^{-7}\ \mathrm{m}^2)$ is the area of a palladium dot. This technique yields a thickness of 1.40 μm. The band gap, which is not well-defined in amorphous materials, was estimated to be $\varepsilon_g \approx 1.8$ eV from optical measurements.

The sample was mounted on a custom-made transistor header, as shown in Figure 4.2. Two of the transistor leads were connected with a spring hook, which simultaneously held the sample in place and made electrical contact to a palladium dot. The voltage bias was

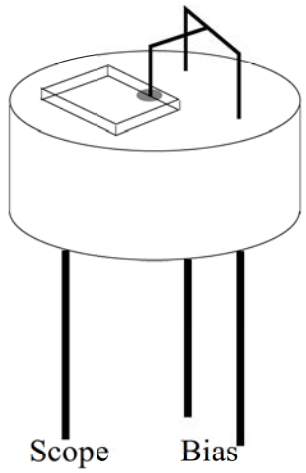

FIGURE 4.2: Sample mounted on a transistor header. A voltage bias was applied to the front contact through a spring hook; the photocurrent was measured from the back contact with an oscilloscope.

connected to one of these leads. The third lead contacted the stainless steel substrate through the transistor body, and was connected to the oscilloscope.

5

RESULTS

5.1 Qualitative observations

A typical photocurrent trace is shown in Figure 5.1. The current falls rapidly in time and looks as if it might have exponential or power law form, save a bump indicated by the arrow. The noise seen at short times is due to the radio-frequency signal emitted by the laser. As discussed in §4.2.1, this signal is picked up by the scope for $t < 500$ ns and rides on top of the photocurrent signal.

From Eqn (3.20), prior to the transit time the current should decrease like $I(t) \propto t^{\alpha-1}$ and hence, plotting the data on logarithmic scales ought to yield a straight line. Figure 5.2 shows the data plotted in Figure 5.1 on logarithmic axes. The current exhibits the so-called dispersive behavior; as predicted, I appears as a straight line until the transit time,[1] indicated by the arrow, beyond which it decays more quickly. This arrow is the same as that in Figure 5.1; apparently the bump becomes a sharp break in the current on logarithmic scales. According to the multiple-trapping model, the pre-transit current decays due to trapping and the post-transit current decays due both to carriers exiting the sample and to trapping of carriers still in the sample. The apparent noise at long times is an effect introduced by the logarithmic scales. At these times the current is approximately zero and small fluctuations due to the oscilloscope's limited resolution are magnified by

[1]The term transit time is used in this chapter to refer to the break in current traces. No physical meaning should be associated with it.

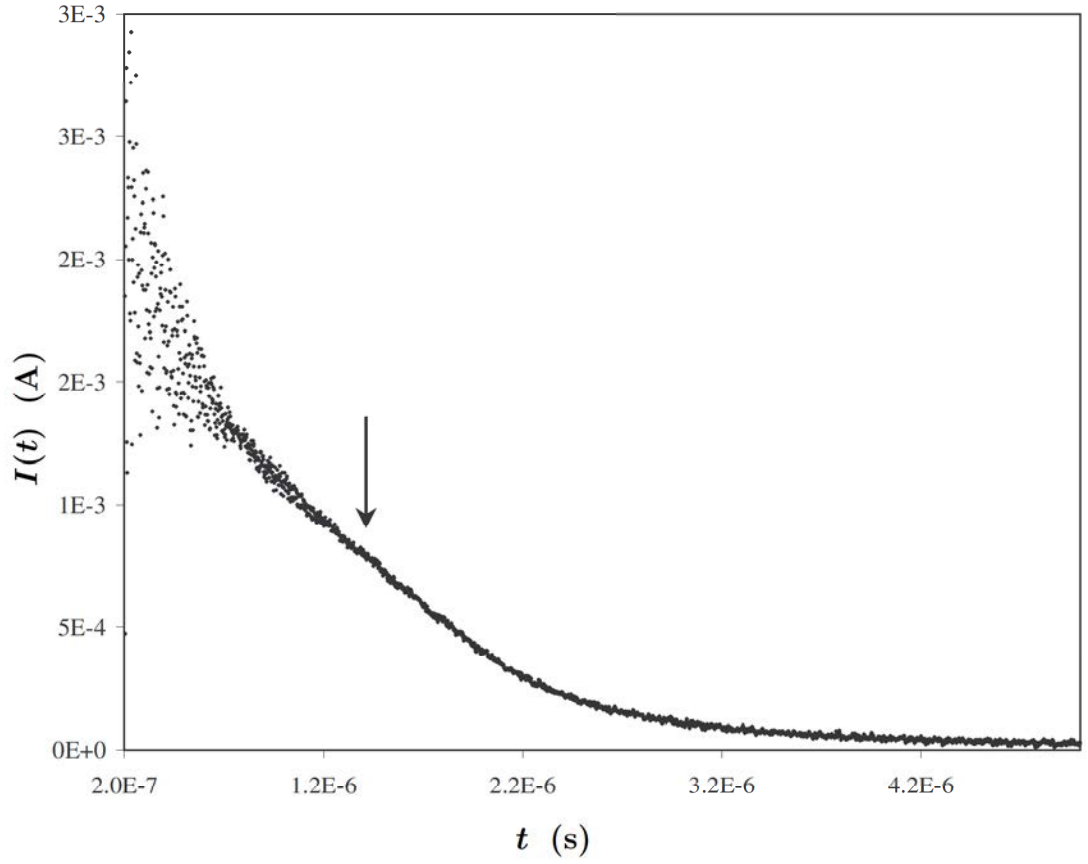

FIGURE 5.1: Typical photocurrent trace. Data were recorded at temperature $T = 170$ K with applied bias $V = 7$ V. The current transient appears to have a shoulder at approximately $t = 1.5 \times 10^{-6}$ s (see arrow).

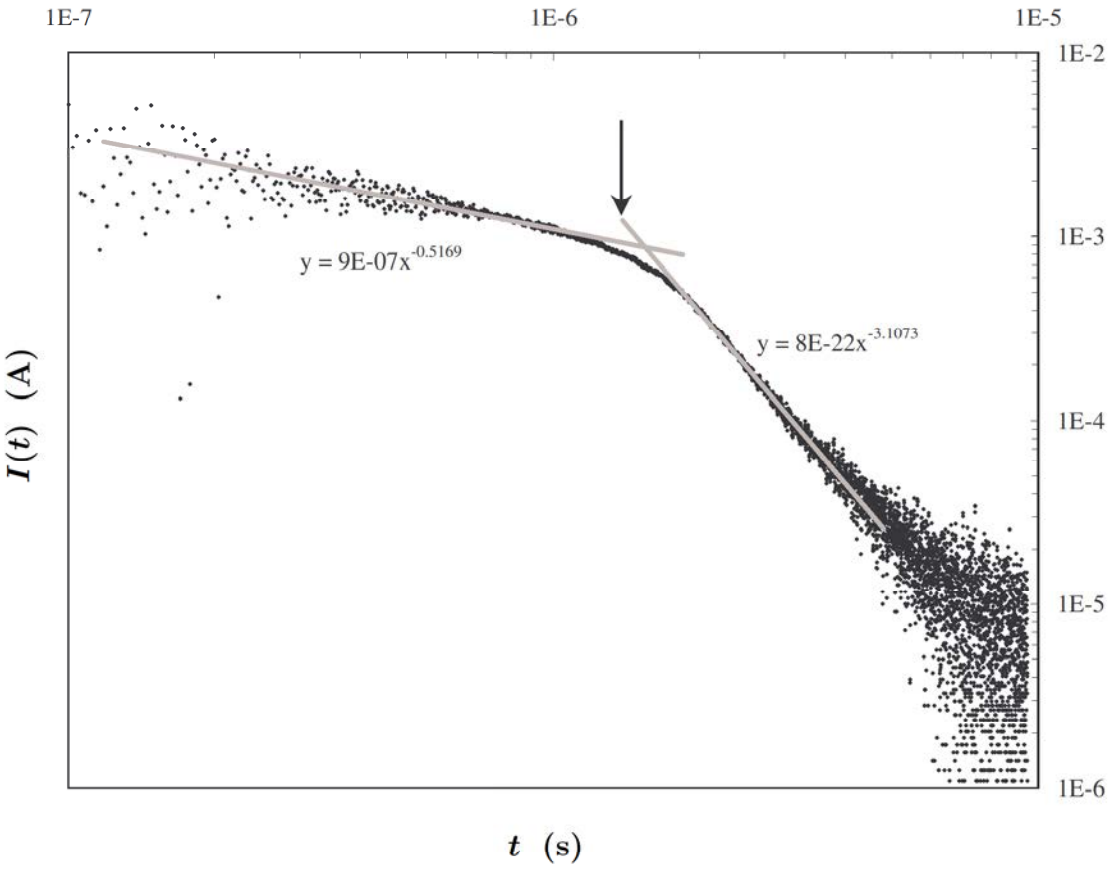

FIGURE 5.2: Typical current trace plotted on logarithmic scales. Data were recorded at temperature $T = 170$ K with applied bias $V = 7$ V. Two straight line regimes are seen, with a distinct break shown by the arrow. This is the signature of dispersive transport. Fitting the pre-transit data to the predicted current, $I(t) \propto t^{\alpha-1}$, yields $\alpha = 0.48$. In some cases it is observed that the long-time current decay obeys $I(t) \propto t^{-\alpha-1}$. This implies that the sum of the pre- and post-transit slopes is -2, which was not observed in this case.

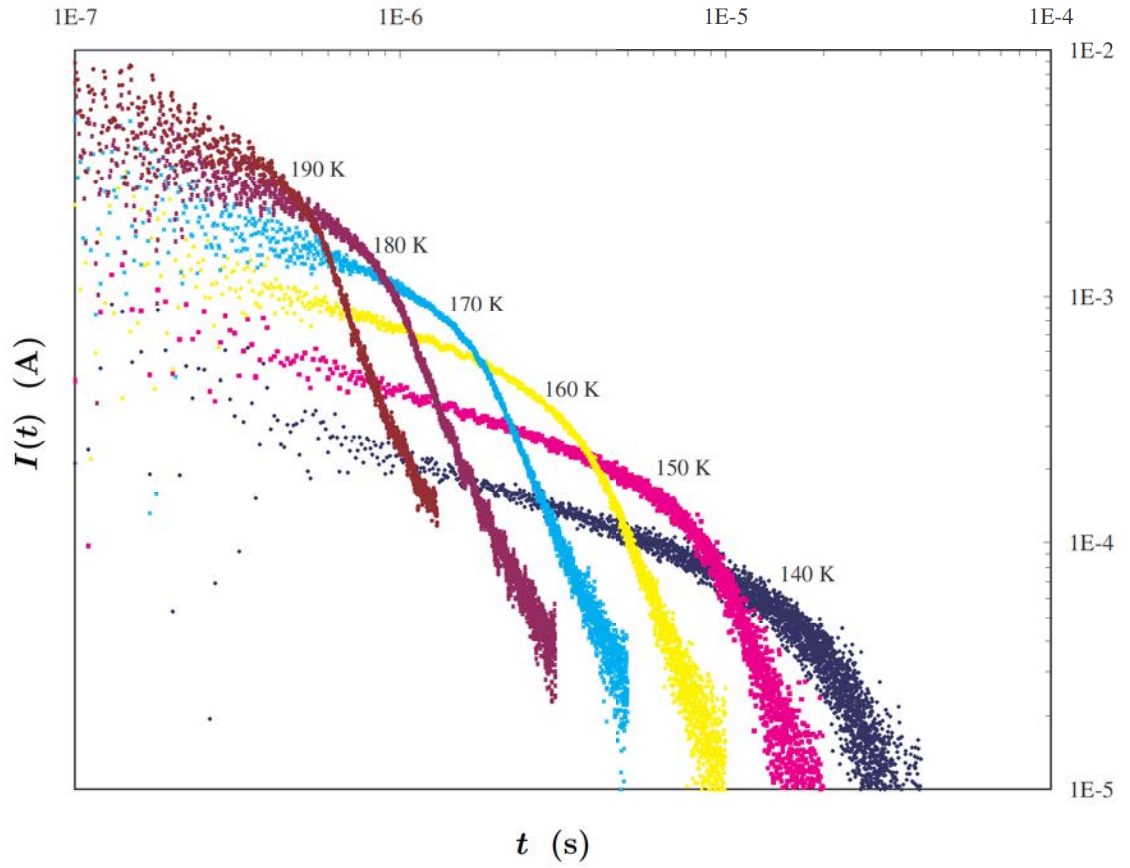

FIGURE 5.3: Photocurrent traces recorded at temperatures $T = 140 - 190$ K with constant applied bias $V = 7$ V. With decreasing temperature, the magnitude of the photocurrent decreases and the transit time increases.

the non-linear axes.

Interesting information can be gleaned simply by observing the relationships between photocurrent transients recorded at different temperatures and applied voltage biases. First, transport has some dependence on temperature. Figure 5.3 displays current traces recorded at various temperatures with constant applied bias.

At higher temperatures, a larger pre-transit current is measured. Though not profound, this is consistent with the multiple-trapping model (Eqn (3.20)). Additionally, the transit time increases with decreasing temperature. This is qualitative support for multiple trapping, which predicts that carriers will take longer to traverse a finite thickness sample at lower temperatures because emission from traps is thermally activated.

Second, Eqn (3.27) predicts that the transit time is not proportional to the applied

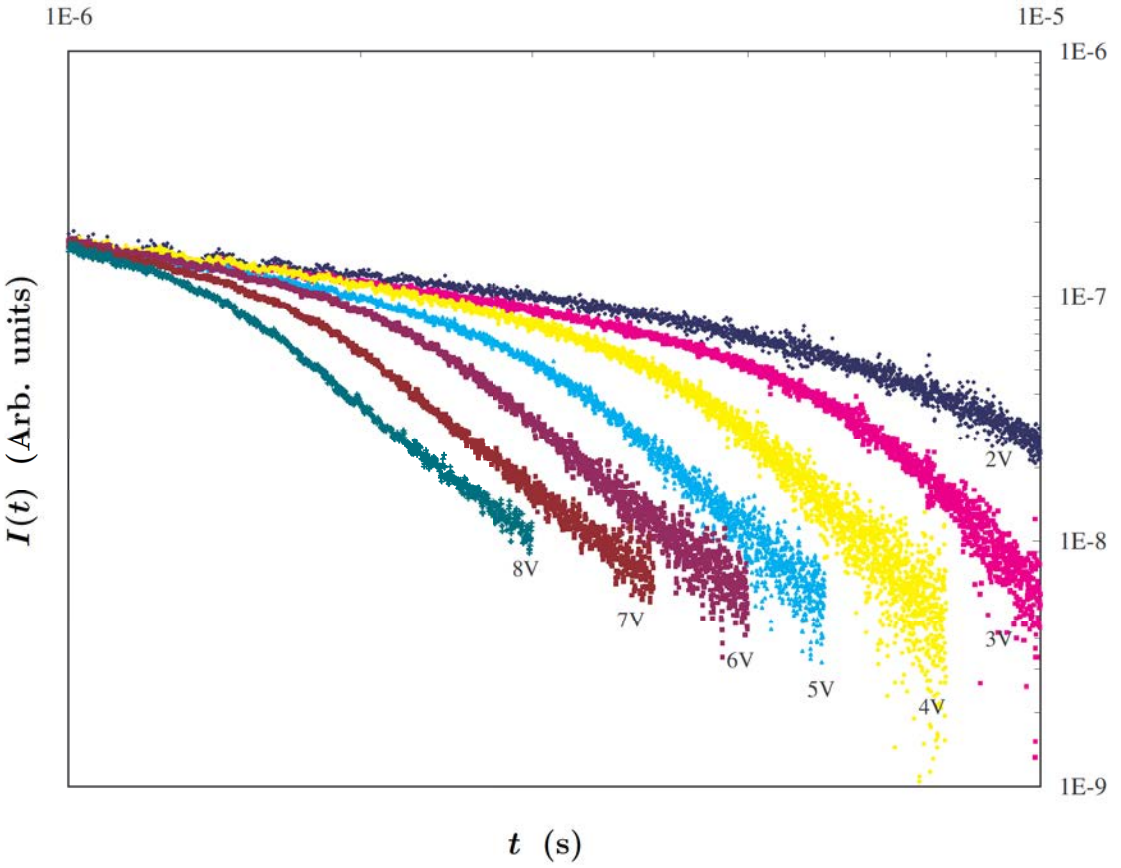

FIGURE 5.4: Photocurrent traces recorded at temperature $T = 170$ K with applied biases $V = 2 - 8$ V. This magnified view of the traces near their transit times shows the non-linear dependence of the transit time on applied electric field. To make this easy to see, the traces have been normalized so that the pre-transit currents of each trace overlap.

electric field. This is seen in Figure 5.4. Note, however, that the magnitude of the current is proportional to the field (Figure 5.5), as anticipated by Eqn (3.20).

5.2 Transient mobility

One of the fundamental quantities of interest is the transient mobility, or velocity of an average carrier per unit electric field at any time prior to the transit time. Note that this is the time regime with which we are primarily concerned; the steep post-transit current decay is an artifact of the sample thickness and tells us nothing about electron transport or the material parameters. To find the transient mobility from the data, we solve Eqn

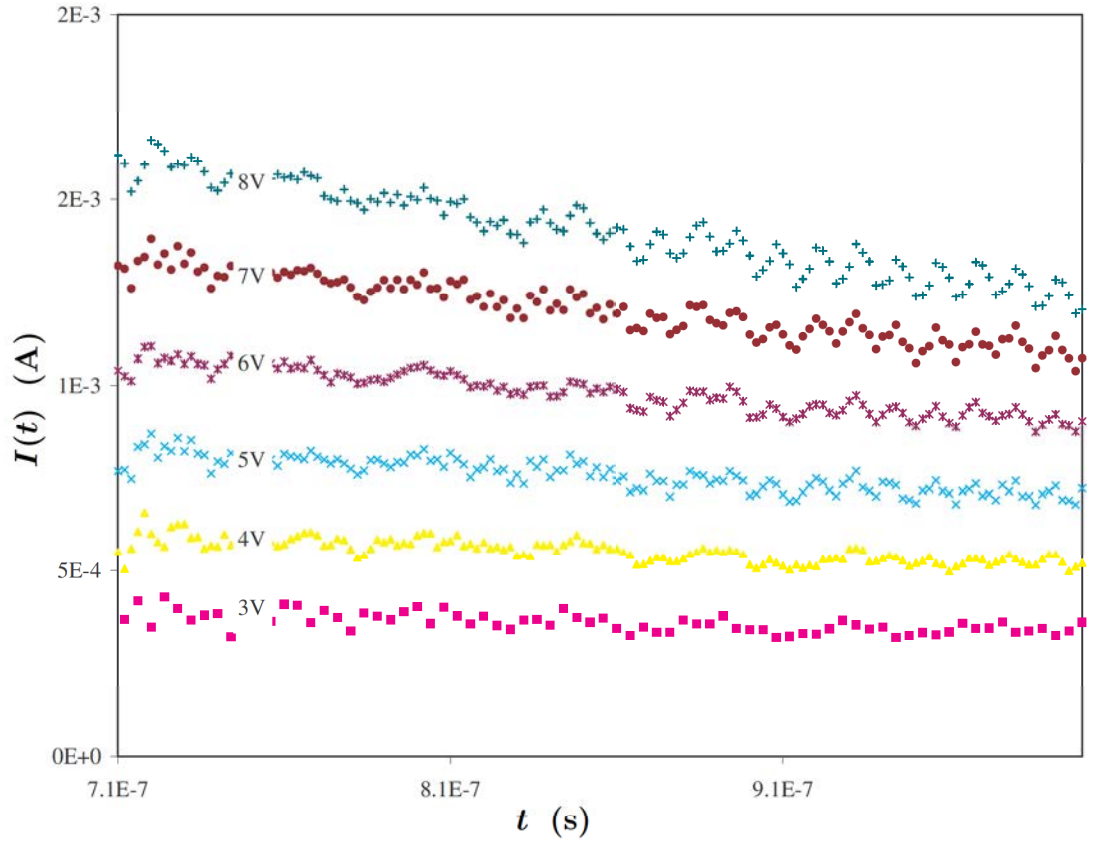

FIGURE 5.5: Magnified view of pre-transit photocurrent traces. These traces were recorded at temperature $T = 170$ K with applied biases $V = 2 - 8$ V. Notice the linear scale. At any given time, an increase in the bias yields an equal increase in the current, indicating that the magnitude of the photocurrent is linear in electric field.

(3.19) for $\mu(t)$:

$$\mu(t) = \frac{d^2}{Q_0 V} I(t), \tag{5.1}$$

where d is the sample thickness, $Q_0 = Ne$ is the total photogenerated charge in the sample, and $E = V/d$ has been used. Apparently all we have to do is normalize the current data from TOF experiments to find the transient mobility!

5.2.1 Finding Q_0

Both d and V are known, but how do we find Q_0? Integrating both sides of Eqn (5.1) with respect to time yields the displaceability (introduced briefly in §3.4):

$$\frac{x(t)}{E} = \frac{d^2}{Q_0 V} Q(t), \tag{5.2}$$

where $Q(t)$ is the charge (I call it the *photocharge*) that has been collected at the back contact since the start of the experiment. Rearranging Eqn (5.2) yields:

$$x(t) = d\frac{Q(t)}{Q_0}, \tag{5.3}$$

and hence, the mean position of the photocarriers is proportional to the fraction of charge collected. At long enough times, nearly all the carriers have completed their transit, $x(t) \to d$, and $Q_0 = Q(t)$.

The photocharge was determined by numerical integration of the photocurrent, and a typical charge trace is shown in Figure 5.6. This trace was calculated from the data plotted in Figures 5.1 and 5.2, and the familiar transit time arrow is shown. As one would anticipate when looking at the current trace, the charge has power law form until the transit time, after which it becomes asymptotic. Q_0 is simply the value of the asymptote.

In Figure 5.7, charge curves at various temperatures with fixed bias are plotted and my estimate of Q_0 is shown. Intuitively, we expect that Q_0 should be independent of both temperature and voltage bias. That is, at long enough times (but not longer than the recombination time) all the photoexcited electrons should complete their transit and

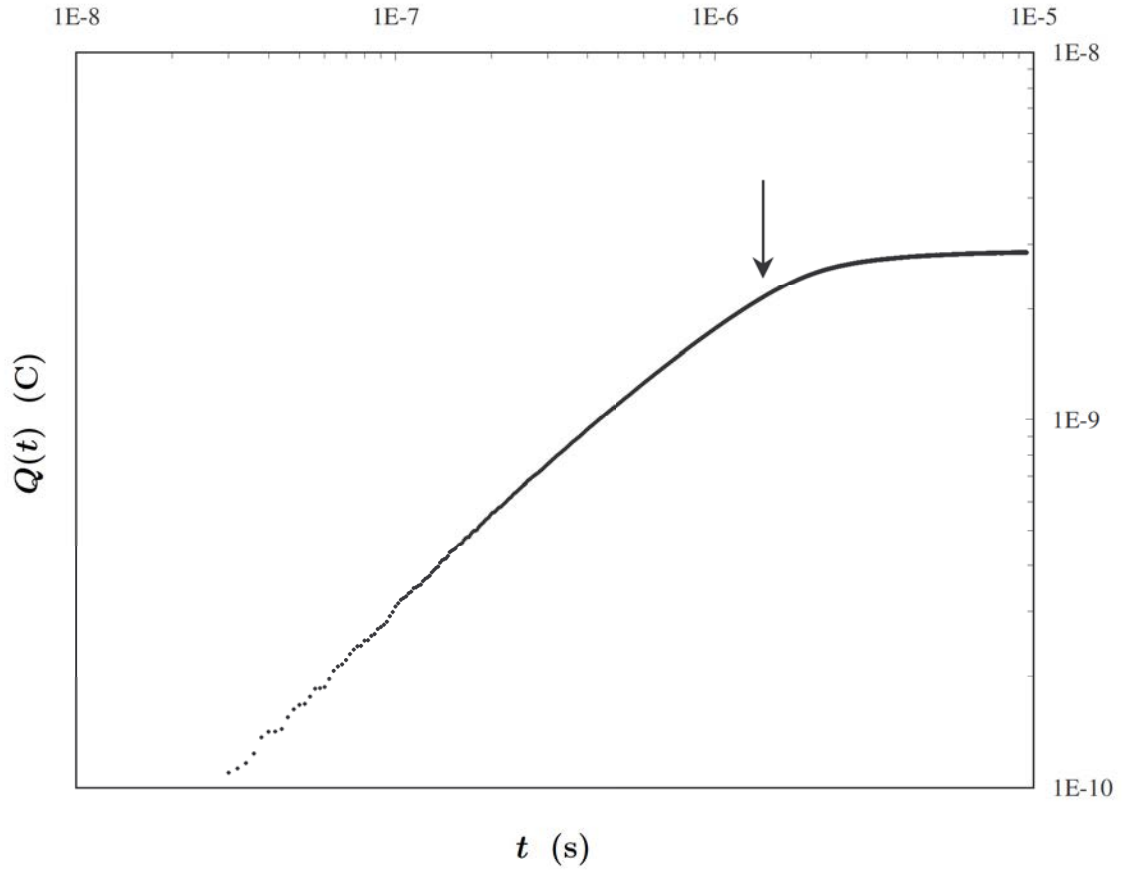

FIGURE 5.6: Photocharge trace determined by numerical integration of photocurrent data recorded at temperature $T = 170$ K with applied bias $V = 7$ V. The charge increases with power law form (it appears as a straight line on the logarithmic scales) until the transit time (indicated by the arrow) at which point it levels off at Q_0.

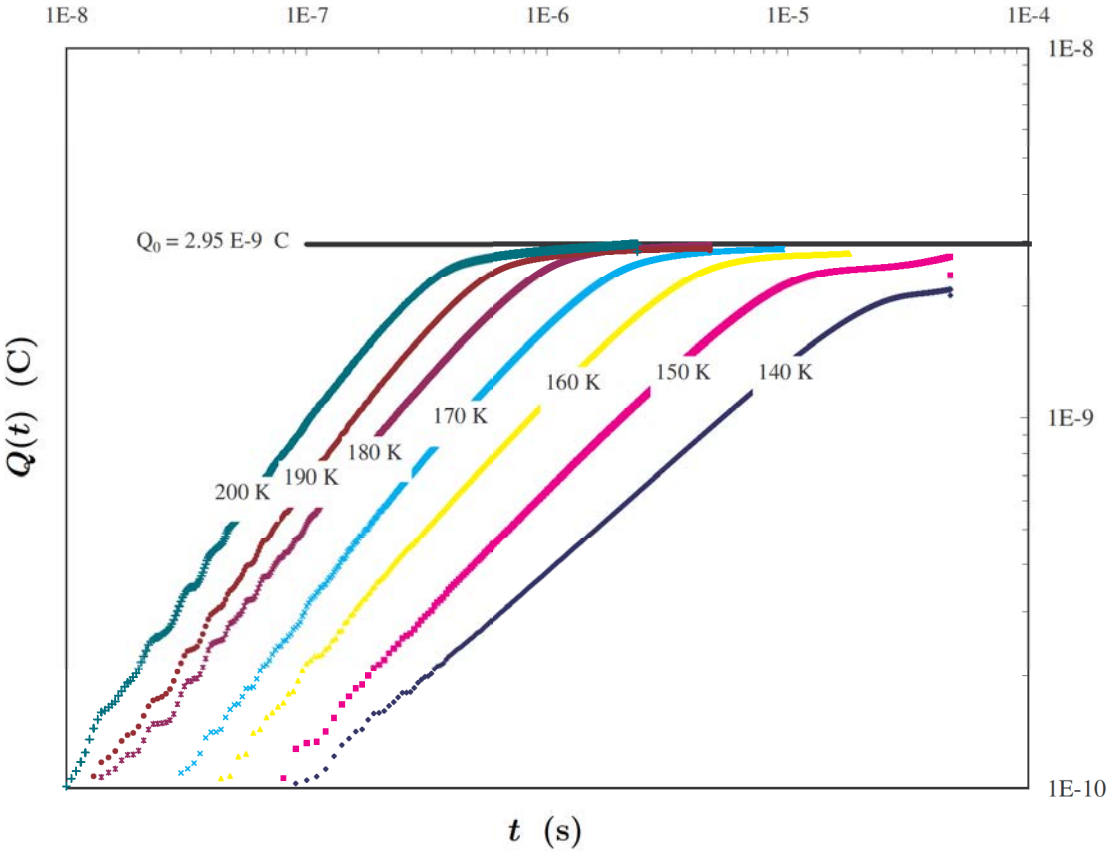

FIGURE 5.7: The total photogenerated charge $Q_0 = 2.95$ nC is estimated from the long-time limit of photocharge traces recorded at temperatures $T = 140 - 200$ K with constant applied bias $V = 7$ V.

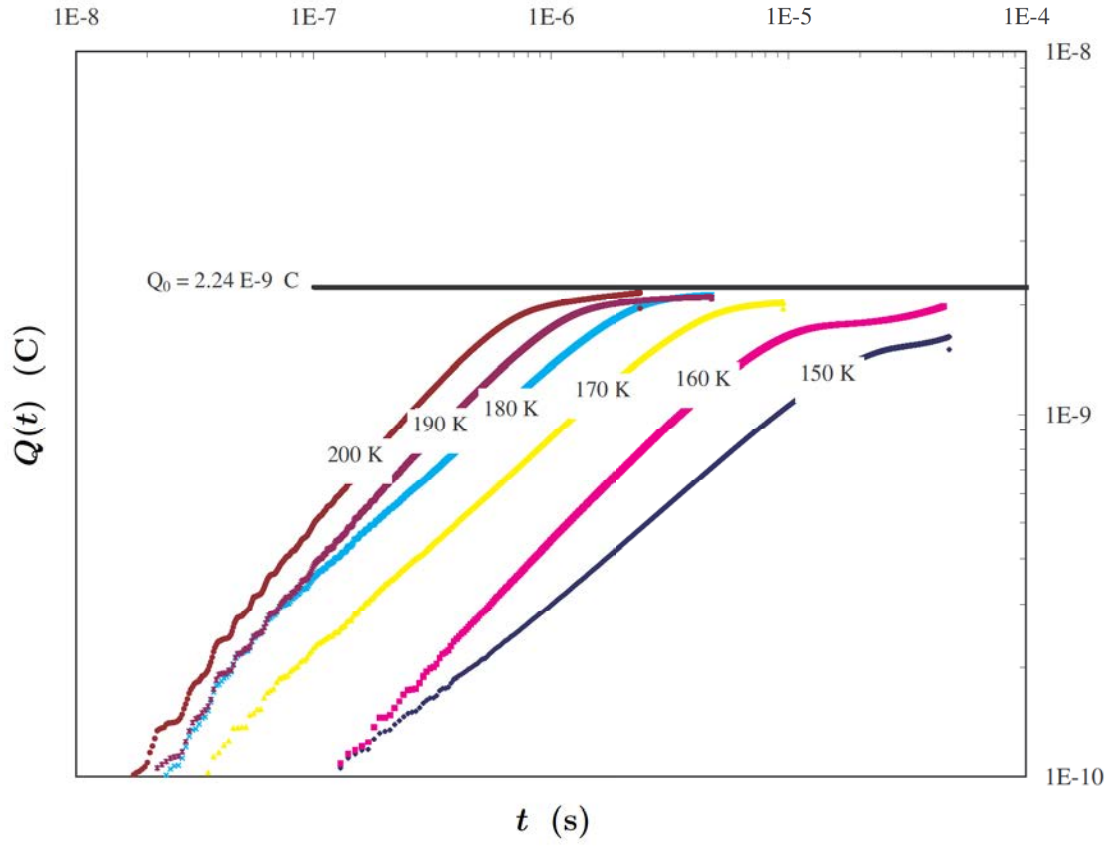

FIGURE 5.8: The total photogenerated charge $Q_0 = -2.24$ nC is estimated from the long-time limit of photocharge traces recorded at temperatures $T = 150 - 200$ K with constant applied bias $V = 4$ V.

be collected no matter what the system parameters are.[2] However, I found that at lower voltages less charge was collected, indicating that Q_0 depends slightly on the applied field. As in Figure 5.7, Figure 5.8 displays charge curves at several temperatures. The plots are the same except that a smaller bias was used to obtain the data shown Figure 5.8. In Figure 5.8, the estimated value of Q_0 is noticeably lower than in Figure 5.7.[3]

[2]Schiff et al. [37] reported this to be the case in similar measurements on a-Si:H.

[3]It may be argued that, given more time, the curves in Figure 5.8 would increase slowly up to $Q_0 \approx 3$ nC as in Figure 5.7, but I do not believe this is true. In general the collected charge levels off quickly after the transit time and will not increase substantially. Regardless, it does not matter much whether Q_0 is constant or variable. Photocurrent is linear in electric field and if the proportionality constant in Eqn (5.2) is chosen correctly, the pre-transit current traces will overlap. For the data presented here, this is achieved by a bias-dependent Q_0.

TABLE 5.1: Estimates of Q_0 from the long-time limit of collected charge curves.

V (V)	Q_0 (nC)
2	1.66
3	1.91
4	2.24
5	2.57
6	2.75
7	2.95
8	3.16

5.2.2 Normalized current traces

The values of Q_0 estimated at each bias and used in Eqn (5.1) to normalize the current traces are displayed in Table 5.1.[4]

The normalized current at $T = 160$ K is shown in Figure 5.9. The pre-transit current traces overlap and define an envelope curve, from which they peel away at their respective transit times. The envelope curve is the transient mobility, fit here with the black line. Crudely, one could determine the velocity of an average photoexcited electron prior to its transit by reading the mobility directly from the fit in Figure 5.9 and multiplying by the electric field.

A more refined method to explicitly determine the velocity of an average electron would be to fit the data to the multiple-trapping model developed in Chapter 3. Using the pre-transit data from each trace, we would have one transient mobility curve at each temperature. Equation (3.13) could then (in principle) be used to fit all of these curves simultaneously. However, there are problems. Equation (3.13) has a complex form and it is not clear how to carry out the fitting procedure. Additionally, at higher temperatures ($T \geq 170$ K), transit times are sufficiently short that the radio-frequency signal emitted by the laser obscures the pre-transit current (Figure 5.10). There is no reason to believe that we can extract meaningful information about transport from the widely dispersed

[4]Surprisingly or not, the relationship between Q_0 and V looks to be roughly linear.

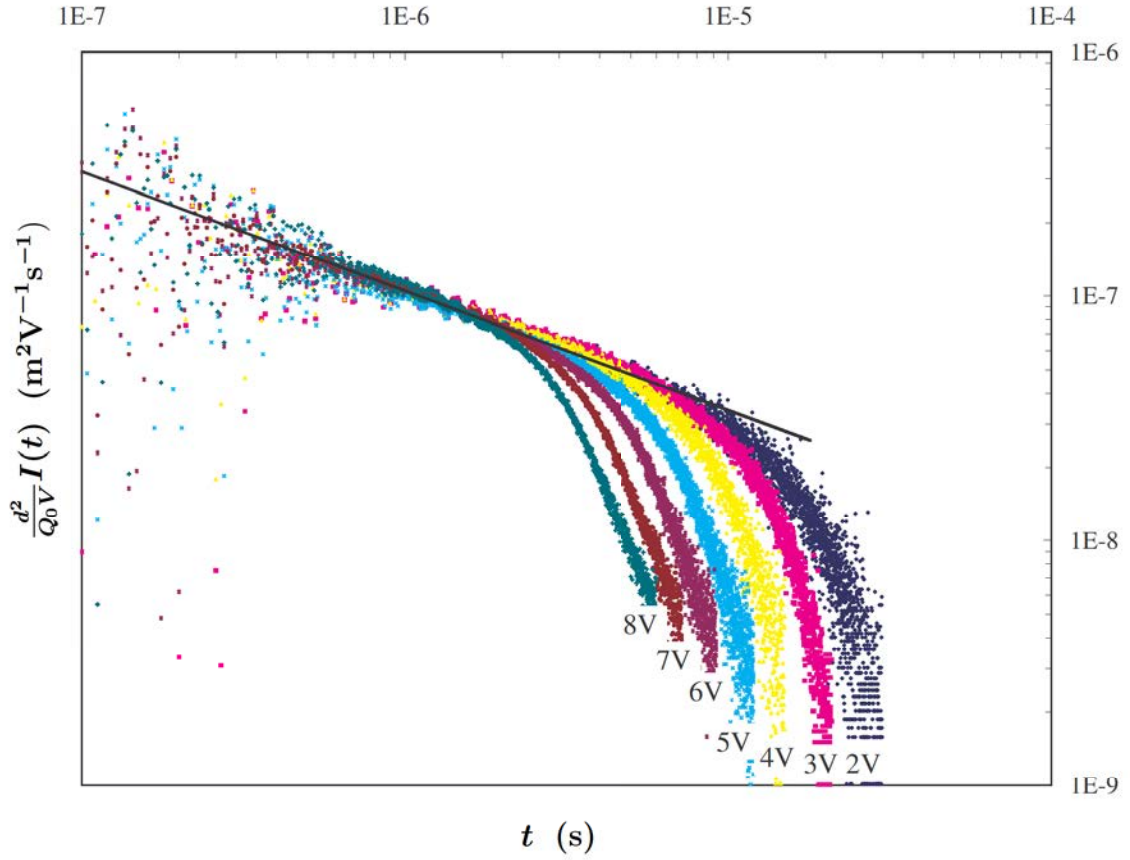

FIGURE 5.9: Normalized current traces at temperature $T = 160$ K with applied biases $V = 2 - 8$ V define the transient mobility envelope curve (Eqn (5.1)).

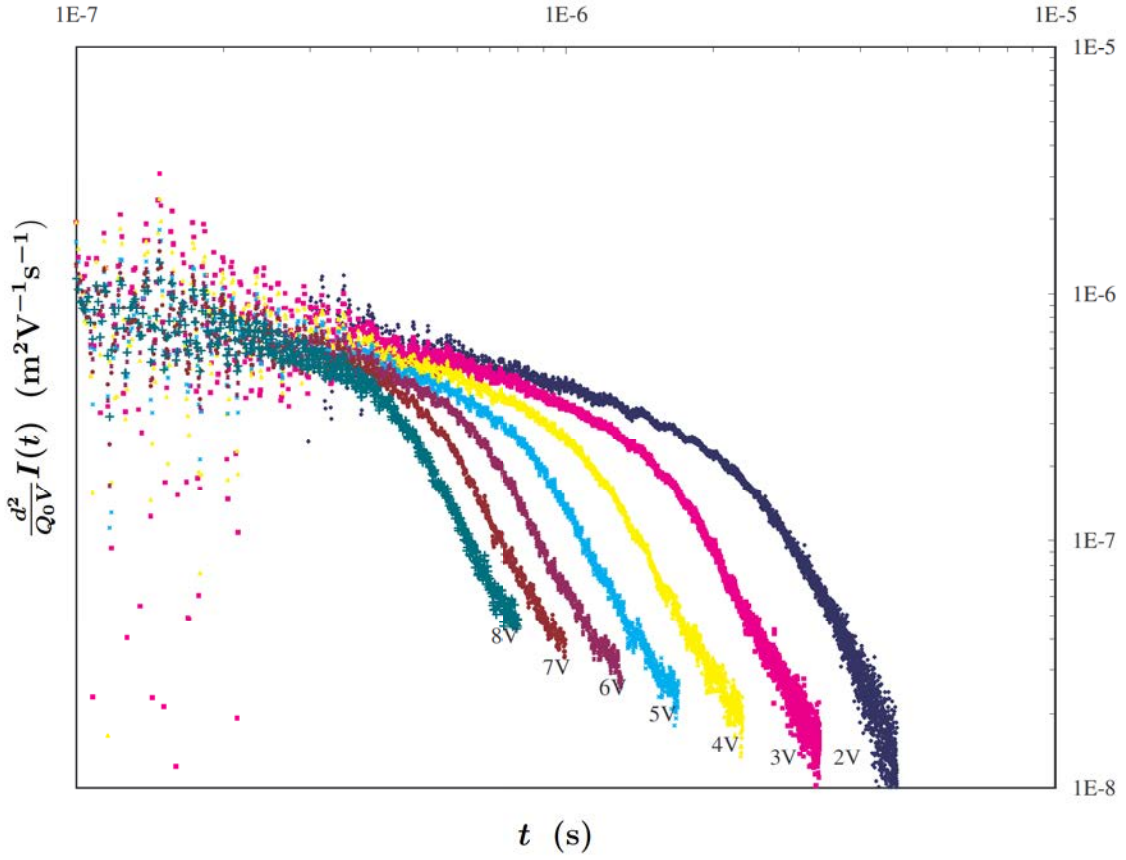

FIGURE 5.10: Normalized current traces at temperature $T = 190$ K with applied biases $V = 2 - 8$ V. Radio-frequency noise emitted by the laser makes it difficult to determine the transient mobility curve.

pre-transit data by fitting it.

5.3 Fitting charge curves

Schiff et al. [54] have proposed a better method for comparing the model to the data using charge curves. According to Eqn (5.2), the displaceability, or average position of the drifting electrons per unit electric field, is obtained from the normalized (pre-transit) charge. Normalized charge curves for several voltage biases at constant temperature are displayed in Figure 5.11. Note that, excepting the 2 V trace, the curves overlap prior to their respective transit times. The envelope, indicated by the black line, is the displaceability curve.

We will fit the multiple-trapping model to displaceability curves at several tempera-

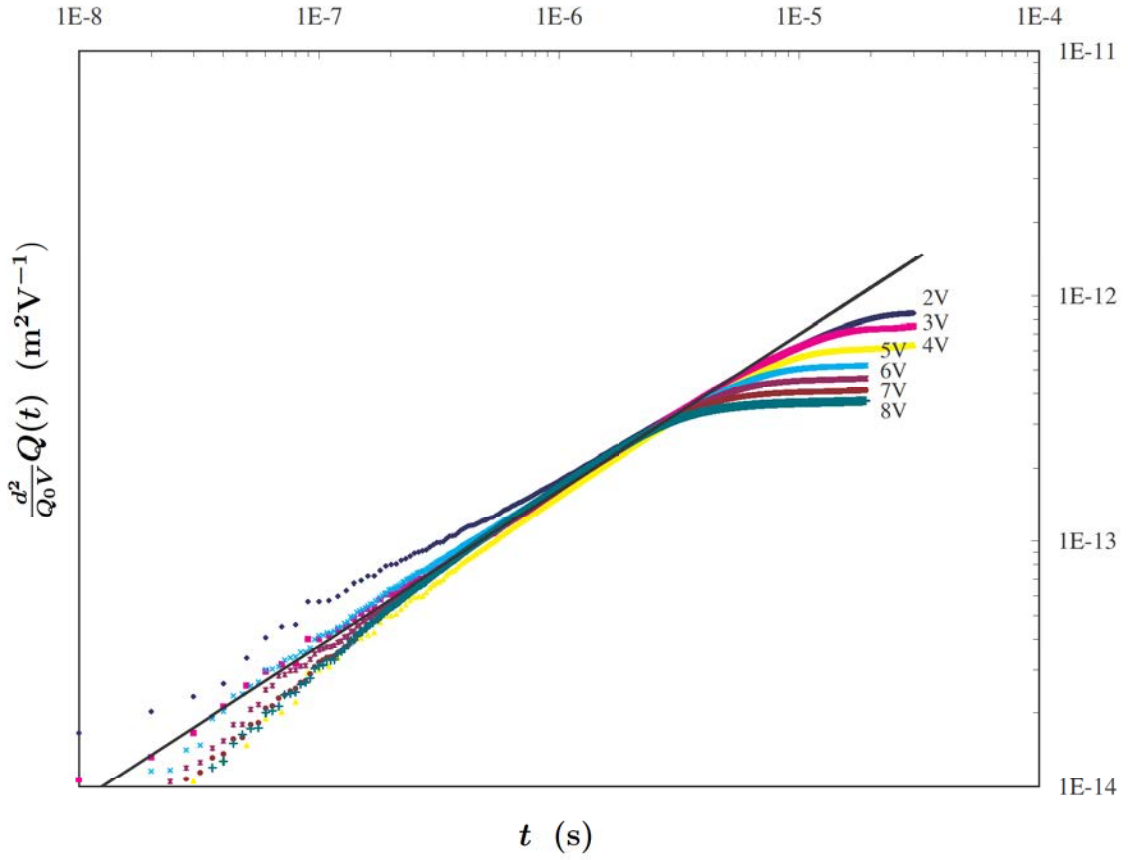

FIGURE 5.11: Normalized charge traces at temperature $T = 160$ K with applied biases $V = 2 - 8$ V define the displaceability envelope curve (Eqn (5.2)).

tures momentarily. First, I will argue that the short-time data for the 2 V trace in Figure 5.11 (and other such deviant curves) should be discarded. It is assumed in the TOF experiment that photogenerated holes are swept out of the sample very quickly and the observed photocurrent is due to electrons only. However, if the applied electric field is small, the holes may not complete their transit before the rise time of the oscilloscope, and a hole current will be measured.[5] In this case, the hole current will add to the electron current since the holes have opposite charge and travel in the opposite direction. This will cause an increase in the collected charge during the time span when the holes were in transit. Such an increase is observed at short times on the 2 V trace in Figure 5.11.

At higher temperatures, the effect I have attributed to hole currents is more easily seen (Figure 5.12). I believe this occurs because faster electron transit times require that the oscilloscope be adjusted to take data on shorter time scales, and on these scales hole transport is easier to observe. Notice, for example, that there are many data points at $t = 10^{-7}$ in Figure 5.12. In Figure 5.11, this time is near the limit of the temporal resolution of the oscilloscope and there are very few points.

Given the argument above, the low-bias charge curves were discarded. The irrelevant post-transit data for each trace were also removed. The remaining data—a family of seven displaceability curves—were fit simultaneously to the multiple-trapping model. It is convenient to work with the displaceability for two reasons. First, the fitting procedure is simple. Second, the displaceability curves are smooth, since the sinusoidal laser noise seen in the photocurrent traces averages to zero when integrated. Note that if we had somehow fit to the noisy normalized current data, we would have never suspected that holes contributed to the low-bias traces. The unwanted data would have been included, and the fit would have been inaccurate.

What form does multiple trapping predict for the displaceability? Using Eqn (3.13),[6]

$$\frac{x(t)}{E} = \int_0^t \mu(t)\ \mathrm{d}t$$

[5] Schiff et al. [41] observed this effect previously.

[6] Ideally we would use the exact form of the transient mobility which includes a factor of $\sin(\pi\alpha)/(\pi\alpha)$; however, the fitting procedure described would not work if this factor were included. It is not worth fretting about its neglect since to second-order approximation this factor is one.

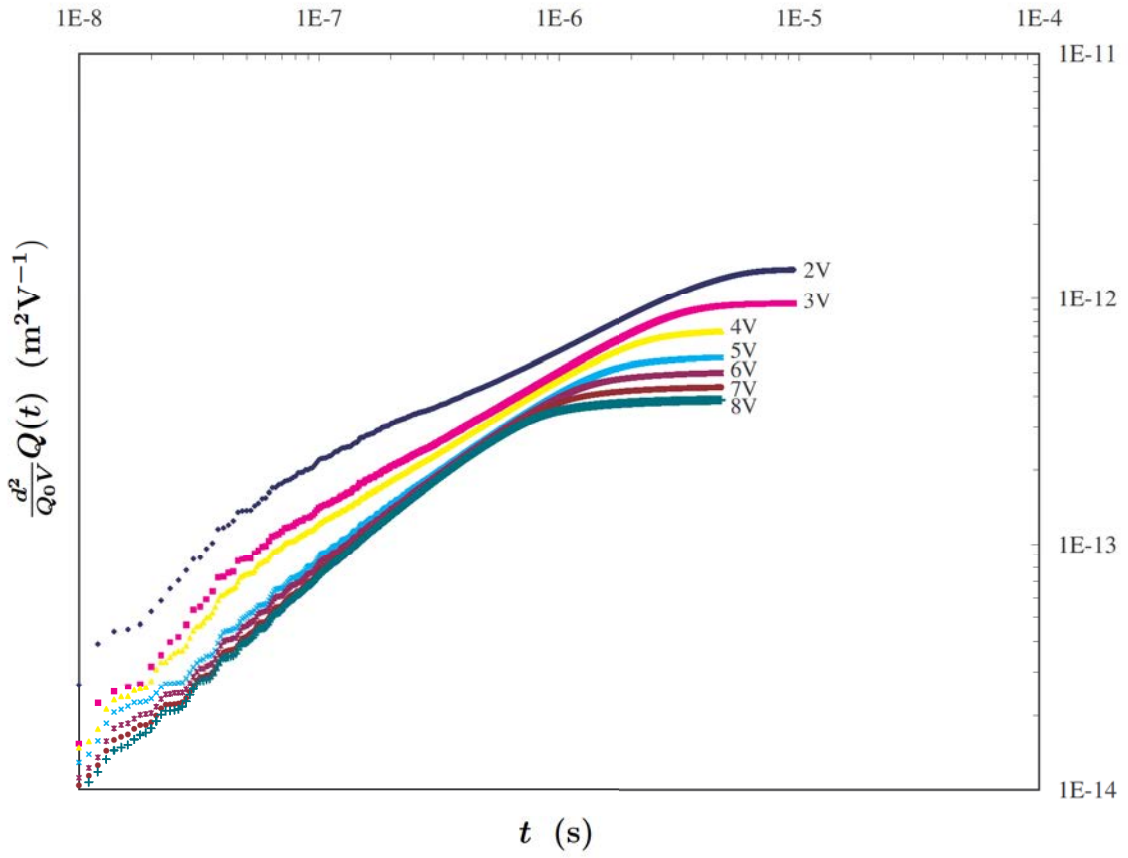

FIGURE 5.12: Normalized charge traces at temperature $T = 180$ K with applied biases $V = 2 - 8$ V. Unexpected additional charge is collected at short times for small applied biases. It is suspected that this additional charge is due to the movement of photoexcited holes.

$$= \mu_0 \int_0^t (\nu t)^{\alpha-1}\, \mathrm{d}t$$
$$= \frac{\mu_0}{\nu}(\nu t)^{\alpha}. \tag{5.4}$$

Or, plugging in $\alpha = T/T_c = kT/\Delta\varepsilon$,

$$\frac{x(t)}{E} = \frac{\mu_0}{\nu}(\nu t)^{kT/\Delta\varepsilon}. \tag{5.5}$$

Taking advantage of the properties of the log function,

$$\begin{aligned}\log\left[\frac{x(t)}{E}\right] &= \log\left[\frac{\mu_0}{\nu}(\nu t)^{kT/\Delta\varepsilon}\right] \\ &= \log\left(\frac{\mu_0}{\nu}\right) + \frac{kT}{\Delta\varepsilon}\log(\nu t) \\ &= \log\left(\frac{\mu_0}{\nu}\right) + \frac{kT}{\Delta\varepsilon}\log(\nu) + \frac{kT}{\Delta\varepsilon}\log(t)\,. \end{aligned} \tag{5.6}$$

This has the form $a + bf_1 + cf_1f_2$ with:

$$a = \log\left(\frac{\mu_0}{\nu}\right) \tag{5.7}$$
$$b = \frac{k}{\Delta\varepsilon}\log(\nu) \tag{5.8}$$
$$c = \frac{k}{\Delta\varepsilon} \tag{5.9}$$

and

$$f_1(t,T) = T \tag{5.10}$$
$$f_2(t,T) = \log(t)\,. \tag{5.11}$$

This form is convenient for a linear least-squares regression: $\log\left[\frac{x(t)}{E}\right]$ has been written as a linear combination of functions of the known variables t and T. Mathematica fit all 25,000 data points simultaneously and returned the parameters a, b, and c that determined the family of functions that best fit the data. Solving Eqns (5.7) to (5.9) yielded the desired physical parameters μ_0, ν, and $\Delta\varepsilon$.

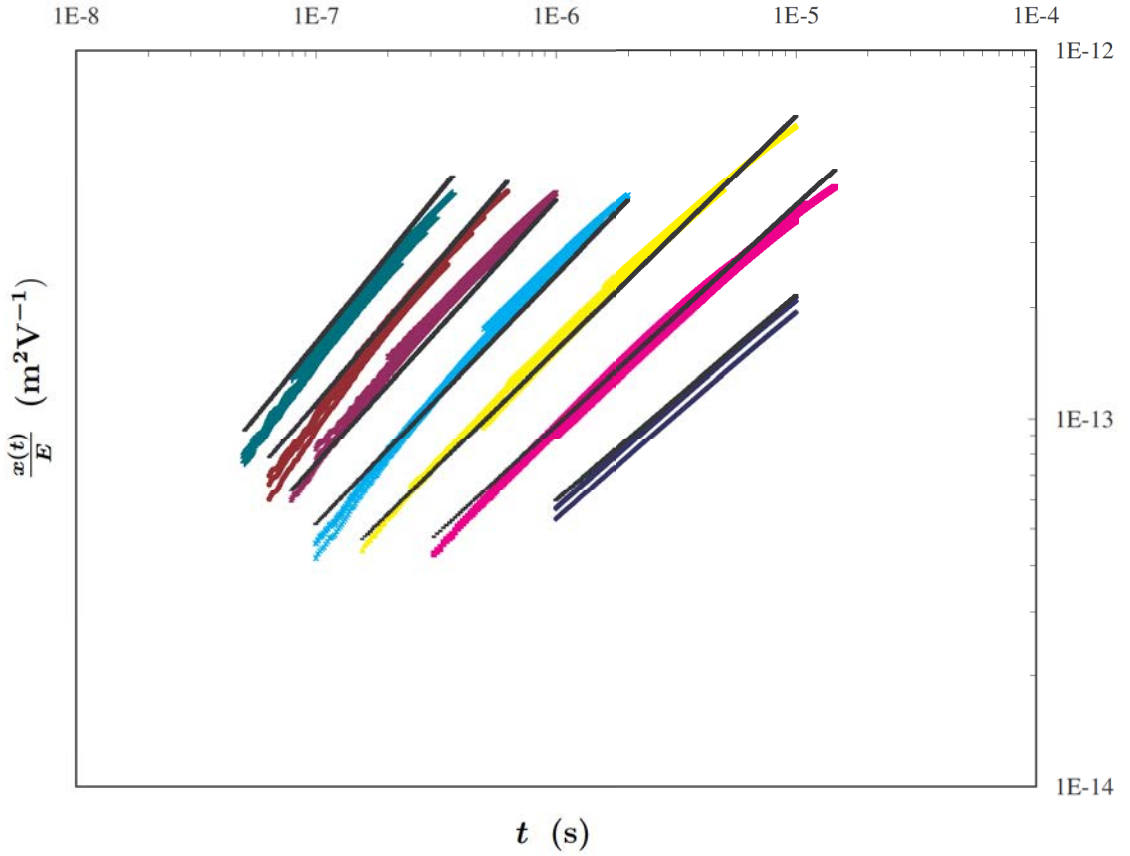

FIGURE 5.13: Displaceability curves at seven temperatures, determined from the pre-transit normalized charge traces, are simultaneously fit with Eqn (5.6). The fit, indicated at each temperature with a black line, is very good.

Figure 5.13 shows the displaceability plots and the corresponding best-fit line. Considering that all seven traces were fit with only three adjustable parameters, the agreement between the data and the multiple-trapping model is quite remarkable. The fit gives $\mu_0 = 0.11$ cm^{2}V^{-1}s^{-1}, $\nu = 1.3 \times 10^{11}$ s^{-1}, and $\Delta\varepsilon = 22$ meV.

These values are consistent with what others [55] have reported: typical values are $\mu_0 = 0.5$ cm^{2}V^{-1}s^{-1} to 5 cm^{2}V^{-1}s^{-1}, $\nu = 10^{11}$ s^{-1} to 10^{12} s^{-1}, and $\Delta\varepsilon = 20$ meV to 40 meV for similar measurements. The $\Delta\varepsilon$ value measured in this thesis is on the low end of the range, indicating that the band tail does not extend far into the gap, and there is less disorder in the sample than is often observed in a-Si:H. It is therefore somewhat surprising that the measured microscopic mobility is smaller than what is typically found, since carriers in a less disorded sample might be expected to have a larger mobility in

the conduction band. However, the discrepancy cannot be reduced significantly by being more or less selective about which data are fit and which are thrown out; I found that any reasonable choice yields the same results. The values assigned to all three parameters are firm.

The microscopic mobility, attempt-to-escape frequency, and band tail width are important in their own right; they give us valuable information about the band tail and the way electrons interact with it during transport. Additionally, the multiple-trapping fit tells us very accurately how the average electron moves through the material in response to an electric field at any time and temperature (within the multiple-trapping regime). The determined values of μ_0, ν, and $\Delta\varepsilon$ may be plugged into Eqn (5.5) to find numerical values of the displaceability and position, Eqn (3.13) to find the transient mobility and velocity, and even Eqns (3.27) and (3.28) to find the transit time and drift mobility in a particular sample for comparison with previously reported values.

6

CONCLUSION

This thesis began with a discussion of photovoltaics, and it ends with one as well. It is time to ask: what does it all mean? How exactly do the band tail parameters of the i-layer in an amorphous solar cell affect the cell's output?

The problem with charge transport in amorphous solar cells is that when low-mobility carriers move through the i-layer, they build up and form a slowly drifting space-charge. This space-charge repels other carriers that are trying to traverse the layer and flow through the external circuit. In essence, there is a traffic jam. According to Eqn (3.13), an increase in either μ_0 or ν, or a decrease in $\Delta\varepsilon$, ought to increase the transient mobility of the carriers and reduce the space-charge effect. This makes sense given the physical meanings of these parameters: if μ_0 is increased the carriers will move faster in the band, if ν is increased the carriers will have the opportunity to escape from traps more often, and if $\Delta\varepsilon$ is decreased there will be fewer (and shallower) traps to immobilize the carriers.

Schiff et al. [2,3] and Tiedje [5] have quantified this effect. They found that the power density generated by an a-Si:H solar cell is proportional to (among other things) ${V_{OC}}^{3/2}$ and ${\mu_{0h}}^{1/4}$, where V_{OC} is the open circuit voltage of the cell and depends on the valence band tail width, and μ_{0h} is the hole microscopic mobility in the valence band. This tells us exactly how the parameters determined from TOF experiments affect the output of photovoltaics.

There is one catch: the parameters used to describe the power density of an a-Si:H cell

all refer to hole transport in the valence band, which was not studied in this thesis. It so happens that the hole transient mobility is significantly smaller than the electron mobility in a-Si:H, which means that hole transport actually limits the power output much more than electron transport.

Perhaps then, the most vital contribution of this thesis to the development of amorphous photovoltaic devices is in the doors it has opened for work yet to come. A reliable TOF experiment has been set up, and measurements with the apparatus have been shown to yield results for electron transport in a-Si:H that are consistent with accepted values. This apparatus may be used to conduct future studies of both electron and hole transport in all sorts of materials.

To that end, I will be continuing this research at Reed this summer. In particular, I plan to perform TOF measurements on nanocrystalline Si:H and Cu(InGa)Se_2 samples. Variants on these relatively new materials are being explored for solar cells, and their charge transport properties are not yet well established.

A

DETAILED BALANCE

This argument, which I owe to Shulman [56], will be easier to follow after reading §3.4.

Suppose the rate at which electrons are trapped in a particular state with energy between ε and $\varepsilon + \mathrm{d}\varepsilon$ is $k_t(\varepsilon)$, and the rate at which they are released from the state is $k_r(\varepsilon)$. Assuming constant capture cross section, $k_t(\varepsilon) = k_t$ is constant. We wish to find $k_r(\varepsilon)$.

Let $\mathrm{d}n_t(\varepsilon)$ be the density (number per unit volume) of trapped electrons between ε and $\varepsilon + \mathrm{d}\varepsilon$, and n_c be the density of electrons in the conduction band. The time rate of change of trapped carriers between ε and $\varepsilon + \mathrm{d}\varepsilon$ is

$$\frac{d}{\mathrm{d}t}\left[\mathrm{d}n_t(\varepsilon)\right] = k_t n_c \left[g(\varepsilon)\mathrm{d}\varepsilon - \mathrm{d}n_t(\varepsilon)\right] - k_r(\varepsilon)\mathrm{d}n_t(\varepsilon), \tag{A.1}$$

and we recognize $g(\varepsilon)\mathrm{d}\varepsilon - \mathrm{d}n_t(\varepsilon)$ as the density of unoccupied traps between ε and $\varepsilon + \mathrm{d}\varepsilon$. The first term in Eqn (A.1) describes the trapping of mobile electrons; the second describes the release of trapped electrons.

At equilibrium, the rate of change of trapped electrons is zero ($\frac{\mathrm{d}}{\mathrm{d}t}\left[\mathrm{d}n_t(\varepsilon)\right] = 0$), and the electron densities are determined by the Boltzmann distribution.[1] As in Chapter 3, let $\varepsilon = 0$ at the conduction mobility edge with positive energy pointing into the gap. Then

[1] We assume that the conduction band and its tail are located at energies several kT above the chemical potential, for which the Fermi distribution approximately reduces to the Boltzmann distribution.

(from Eqn (2.6)),

$$\begin{aligned} \mathrm{d}n_t(\varepsilon) &= g(\varepsilon) f_n(\varepsilon)\ \mathrm{d}\varepsilon \\ &\approx g_0\ e^{-\varepsilon/kT_c}\ e^{-(\mu-\varepsilon)/kT}\ \mathrm{d}\varepsilon. \end{aligned} \tag{A.2}$$

Recalling that the assumed density of states in the conduction band is $g\varepsilon = g_0$, Eqn (2.8) gives:

$$\begin{aligned} n_c &= \int_{\varepsilon_c}^{\varepsilon_{c\,max}} g(\varepsilon) f_n(\varepsilon)\ \mathrm{d}\varepsilon \\ &\approx \int_{-\infty}^{0} g(\varepsilon)\, e^{-(\mu-\varepsilon)/kT}\ \mathrm{d}\varepsilon \\ &= g_0 kT\ e^{-\mu/kT}. \end{aligned} \tag{A.3}$$

Now, returning to Eqn (A.1), we can find the release rate:

$$\begin{aligned} k_r(\varepsilon) &= k_t n_c \left[\frac{g(\varepsilon)\mathrm{d}\varepsilon}{\mathrm{d}n_t(\varepsilon)} - 1\right] \\ &\approx k_t\ g_0 kT\ e^{-\mu/kT} \left[\frac{g_0\ e^{-\varepsilon/kT_c}\ \mathrm{d}\varepsilon}{g_0\ e^{-\varepsilon/kT_c}\ e^{-(\mu-\varepsilon)/kT}\ \mathrm{d}\varepsilon} - 1\right] \\ &= k_t\ g_0 kT\ e^{-\mu/kT} \left[e^{(\mu-\varepsilon)/kT} - 1\right] \\ &= k_t\ g_0 kT \left[e^{-\varepsilon/kT} - e^{-\mu/kT}\right]. \end{aligned}$$

For states in the band tail, $\varepsilon \ll \mu$ and the second term in square brackets can be neglected:

$$k_r(\varepsilon) \approx k_t\ g_0 kT\ e^{-\varepsilon/kT}.$$

The factor multiplying the exponential function varies much more slowly with temperature than the exponential, and can be regarded as constant. Call it ν. Then,

$$k_r(\varepsilon) \approx \nu\ e^{-\varepsilon/kT}.$$

Hence, the release time from a state with energy between ε and $\varepsilon + \mathrm{d}\varepsilon$ is

$$\begin{aligned} t_r(\varepsilon) &= 1/k_r(\varepsilon) \\ &= \frac{1}{\nu}\, e^{\,\varepsilon/kT}. \end{aligned} \tag{A.4}$$

REFERENCES

[1] J. H. Scaff, H. C. Theuerer, and E. E. Schumacher. P-type and n-type silicon and the formation of the photovoltaic barrier in silicon ingots. *Transactions of the American Institute of Mining and Metallurgical Engineers*, 185(6):383–388, 1949.

[2] E. A. Schiff. Low-mobility solar cells: a device physics primer with application to amorphous silicon. *Solar Energy Materials and Solar Cells*, 78(1-4):567–595, 2003.

[3] K. Zhu, J. Yang, W. Wang, E. A. Schiff, J. Liang, and S. Guha. Bandtail limits to solar conversion efficiencies in amorphous silicon solar cells. *Materials Research Society Symposium Proceedings*, 762:A.3.2.1–A.3.2.6, 2003.

[4] R. van Overstraeten and R. P. Mertens. *Physics, technology, and use of photovoltaics.* Modern energy studies. A. Hilger, Boston, 1986.

[5] T. Tiedje. Band tail recombination limit to the output voltage of amorphous-silicon solar-cells. *Applied Physics Letters*, 40(7):627–629, 1982.

[6] H. J. Möller. *Semiconductors for solar cells.* The Artech House optoelectronics library. Artech House, Boston, 1993.

[7] J. R. Haynes and W. Shockley. Investigation of hole injection in transistor action. *Physical Review*, 75(4):691, 1949.

[8] J. R. Haynes and W. Shockley. The mobility and life of injected holes and electrons in germanium. *Physical Review*, 81(5):835–843, 1951.

[9] J. R. Haynes and W. C. Westphal. The drift mobility of electrons in silicon. *Physical Review*, 85(4):680, 1952.

[10] M. B. Prince. Drift mobilities in semiconductors: Germanium. *Physical Review*, 92(3):681–687, 1953.

[11] M. B. Prince. Drift mobilities in semiconductors: Silicon. *Physical Review*, 93(6):1204–1206, 1954.

[12] H. V. Keer. *Principles of the solid state*. J. Wiley and Sons, New York, 1993.

[13] N. W. Ashcroft and N. D. Mermin. *Solid State Physics*. W. B. Saunders, Philadelphia, college edition, 1976.

[14] R. Zallen. *The physics of amorphous solids*. Wiley, New York, 1983.

[15] R. A. Street. *Hydrogenated amorphous silicon*. Cambridge solid state science series. Cambridge University Press, New York, 1991.

[16] K. W. Böer. *Survey of semiconductor physics*. Van Nostrand Reinhold, New York, 1990.

[17] M. Shur. *Physics of semiconductor devices*. Prentice-Hall series in solid state physical electronics. Prentice Hall, Englewood Cliffs, 1990.

[18] A. C. Smith, J. F. Janak, and R. B. Adler. *Electronic conduction in solids*. McGraw-Hill physical and quantum electronics series. McGraw-Hill, New York,, 1967.

[19] D. L. Staebler and C. R. Wronski. Reversible conductivity changes in discharge-produced amorphous si. *Applied Physics Letters*, 31(4):292–294, 1977.

[20] cwx.prenhall.com/bookbind/pubbooks/hillchem3. Website, 2002.

[21] W. van Sark. www.fys.ruu.nl/∼vansark/pic. Website, 2002.

[22] W. J. Halloway. Fabrication and characterization of thin film copper indium diselenide. Master's thesis, Reed College, 1998.

[23] P. W. Anderson. Absence of diffusion in certain random lattices. *Physical Review*, 109(5):1492–1505, 1958.

[24] J. M. Marshall. Carrier diffusion in amorphous-semiconductors. *Reports on Progress in Physics*, 46(10):1235–1282, 1983.

[25] J. Orenstein, M. A. Kastner, and V. Vaninov. Transient photoconductivity and photoinduced optical-absorption in amorphous-semiconductors. *Philosophical Magazine B*, 46(1):23–62, 1982.

[26] G. Pfister and H. Scher. Dispersive (non-gaussian) transient transport in disordered solids. *Advances in Physics*, 27(5):747–798, 1978.

[27] T. Tiedje. Time-resolved charge transport in hydrogenated amorphous silicon. *Topics in Applied Physics*, 56:261–300, 1984.

[28] H. Scher and E. W. Montroll. Anomalous transit-time dispersion in amorphous solids. *Physical Review B*, 12(6):2455–2477, 1975.

[29] J. Noolandi. Multiple-trapping model of anomalous transit-time dispersion in a-se. *Physical Review B*, 16(10):4466–4473, 1977.

[30] F. W. Schmidlin. Theory of trap-controlled transient photoconduction. *Physical Review B*, 16(6):2362–2385, 1977.

[31] J. Orenstein and M. Kastner. Photocurrent transient spectroscopy—measurement of the density of localized states in a-as_2se_3. *Physical Review Letters*, 46(21):1421–1424, 1981.

[32] T. Tiedje and A. Rose. A physical interpretation of dispersive transport in disordered semiconductors. *Solid State Communications*, 37(1):49–52, 1981.

[33] E. Abrahams, P. W. Anderson, D. C. Licciardello, and T. V. Ramakrishnan. Scaling theory of localization: Absence of quantum diffusion in two dimensions. *Physical Review Letters*, 42(10):673–676, 1979.

[34] S. Aljishi, J. D. Cohen, S. Jin, and L. Ley. Band tails in hydrogenated amorphous-silicon and silicon-germanium alloys. *Physical Review Letters*, 64(23):2811–2814, 1990.

[35] T. Tiedje, C. R. Wronski, B. Abeles, and J. M. Cebulka. Electron transport in hydrogenated amorphous silicon: Drift mobility and junction capacitance. *Solar Cells*, 2:301–318, 1980.

[36] T. Tiedje. *Information about Band-Tail States from Time-of-Flight Experiments*, chapter 6, pages 207–238. Academic Press, Orlando, 1984.

[37] Q. Wang, H. Antoniadis, E. A. Schiff, and S. Guha. Electron-drift-mobility measurements and exponential conduction-band tails in hydrogenated amorphous silicon-germanium alloys. *Physical Review B*, 47(15):9435–9448, 1993.

[38] A. M. Johnson, D. H. Auston, P. R. Smith, J. C. Bean, J. P. Harbison, and A. C. Adams. Picosecond transient photocurrents in amorphous-silicon. *Physical Review B*, 23(12):6816–6819, 1981.

[39] C. Longeaud and R. Vanderhaghen. Determination of the density of states of the conduction-band tail in amorphous materials - application to a-si$_{1-X}$ge$_x$:h alloys. *Philosophical Magazine B*, 61(2):277–291, 1990.

[40] T. Tiedje, J.M. Cebulka, D.L. Morel, and B. Abeles. Evidence for exponential band tails in amorphous silicon hydride. *Physical Review Letters*, 46(21):1425–1428, 1981.

[41] S. Dinca, G. Ganguly, Z. Lu, E. A. Schiff, V. Vlahos, C. R. Wronski, and Q. Yuan. Hole drift-mobility measurements in contemporary amorphous silicon. *Materials Research Society Symposium Proceedings*, 762:A.7.1.1–A.7.1.6, 2003.

[42] J. M. Marshall, R. A. Street, and M. J. Thompson. Electron-drift mobility in amorphous si:h. *Philosophical Magazine B*, 54(1):51–60, 1986.

[43] C. E. Nebel and G. H. Bauer. Tail-state distribution and trapping probability in a-si:h investigated by time-of-flight experiments and computer-simulations. *Philosophical Magazine B*, 59(4):463–479, 1989.

[44] V. I. Arkhipov and A. I. Rudenko. Anomalous charge transport in amorphous semiconductors. *Soviet Physics-Semiconductors*, 13(7):1352–1358, 1979.

[45] Z. Vardenay and J. Tauc. Hot-carriers thermalization in amorphous silicon. *Physical Review Letters*, 46(18):1223–1226, 1981.

[46] M. A. Parker and E. A. Schiff. Anisotropic drift mobility in hydrogenated amorphous-silicon. *Physical Review B*, 37(17):10426–10428, 1988.

[47] H. Antoniadis and E. A. Schiff. Isotropy of drift mobilities in hydrogenated amorphous-silicon. *Physical Review B*, 44(8):3627–3637, 1991.

[48] T. Tiedje, B. Abeles, D.L. Morel, T.D. Moustakas, and C.R. Wronski. Electron drift mobility in hydrogenated a-si. *Applied Physics Letters*, 36(8):695–697, 1980.

[49] H. Fritzsche. *Amorphous silicon and related materials.* Advances in disordered semiconductors. World Scientific, Teaneck, 1989.

[50] W.E. Spear. Drift mobility techniques for the study of electrical tranport properties in insulating solids. *Journal of Non-Crystalline Solids*, 1:197–214, 1969.

[51] H. Antoniadis and E. A. Schiff. Transient photocharge measurements and electron-emission from deep levels in undoped a-si:h. *Physical Review B*, 46(15):9482–9492, 1992.

[52] H. Antoniadis and E. A. Schiff. Nonlinear photocarrier drift in hydrogenated amorphous silicon-germanium alloys. *Physical Review B*, 43(17):13957–13966, 1991.

[53] S. Adashi. *Optical Constants of Crystalline and Amorphous Semiconductors: Numerical Data and Graphical Information.* Kluwer Academic Publishers, Norwell, 1999.

[54] Q. Gu, Q. Wang, E. A. Schiff, Y. M. Li, and C. T. Malone. Hole drift mobility measurements in amorphous silicon-carbon alloys. *Journal of Applied Physics*, 76(4):2310–2315, 1994.

[55] E. A. Schiff. Drift-mobility measurements and mobility edges in disordered silicons. *Journal of Physics-Condensed Matter*, 16(44):S5265–S5275, 2004.

[56] R. G. Shulman. Hole trapping in germanium bombarded by high-energy electrons. *Physical Review*, 102(6):1451–1455, 1956.